Heterogeneous oxidation catalysis on ruthenium: bridging the pressure and materials gaps and beyond

2008 J. Phys.: Condens. Matter 20 184017

(http://iopscience.iop.org/0953-8984/20/18/184017)

J. Phys.: Condens. Matter **20** (2008) 184017 (23pp) doi:10.1088/0953-8984/20/18/184017

Heterogeneous oxidation catalysis on ruthenium: bridging the pressure and materials gaps and beyond

J Assmann[1], V Narkhede[1], N A Breuer[1], M Muhler[1,4], A P Seitsonen[2,4], M Knapp[3], D Crihan[3], A Farkas[3], G Mellau[3] and H Over[3,4]

[1] Lehrstuhl für Technische Chemie, Ruhr-Universität Bochum, D-44780 Bochum, Germany
[2] IMPMC, CNRS and Université Pierre et Marie Curie 4 place Jussieu, case 115 F-75252 Paris, France
[3] Physikalisch-Chemisches Institut, Justus-Liebig-Universität, Heinrich-Buff-Ring 58, D-35392 Gießen, Germany

E-mail: muhler@techem.rub.de, ari.p.seitsonen@iki.fi and herbert.over@phys.chemie.uni-giessen.de

Received 27 September 2007, in final form 20 November 2007
Published 17 April 2008
Online at stacks.iop.org/JPhysCM/20/184017

Abstract
It is shown that both the materials and the pressure gaps can be bridged for ruthenium in heterogeneous oxidation catalysis using the oxidation of carbon monoxide as a model reaction. Polycrystalline catalysts, such as supported Ru catalysts and micrometer-sized Ru powder, were compared to single-crystalline ultrathin RuO_2 films serving as model catalysts. The microscopic reaction steps on RuO_2 were identified by a combined experimental and theoretical approach applying density functional theory. Steady-state CO oxidation and transient kinetic experiments such as temperature-programmed desorption were performed with polycrystalline catalysts and single-crystal surfaces and analyzed on the basis of a microkinetic model. Infrared spectroscopy turned out to be a valuable tool allowing us to identify adsorption sites and adsorbed species under reaction conditions both for practical catalysts and for the model catalyst over a wide temperature and pressure range. The close interplay of the experimental and theoretical surface science approach with the kinetic and spectroscopic research on catalysts applied in plug–flow reactors provides a synergistic strategy for improving the performance of Ru-based catalysts. The most active and stable state was identified with an ultrathin RuO_2 shell coating a metallic Ru core. The microscopic processes causing the structural deactivation of Ru-based catalysts while oxidizing CO have been identified.

Contents

[4] Authors to whom any correspondence should be addressed.

1. Introduction

The science and the technology of catalysis are of fundamental importance for the European and in particular for the German economy [1]. About 80% of all technical chemicals are manufactured by utilizing catalysts. So far, industrial catalysts have been mostly invented by trial and error methods. The improvement of existing catalysts or the identification of new and better catalysts leading to the next generation of industrial catalysts is envisioned to rely on the rational catalyst design which is based on the understanding of the complete catalytic reaction system on the atomic scale.

The chemistry of industrially working catalysts is, however, far too complex to permit a comprehensive understanding of all the involved processes and reaction steps on the atomic scale. This problem calls for idealization of the experimental conditions including the use of model catalysts with low structural complexity such as single-crystalline surfaces and to investigate them under well-controlled conditions such as ultrahigh vacuum (UHV) [2]. The trade-off for this so-called surface science approach is the inevitable emergence of a pressure gap (10^{-13} bar versus 100 bar) and of a materials gap (single crystal versus supported nanometer-sized particles), by which elementary reaction steps, reaction intermediates, the chemical state of the catalyst, etc. identified under well-defined conditions may not be transferable or relevant to realistic reaction conditions.

The relevance of surface science studies to realistic catalytic systems is therefore subject of an ongoing debate. For some reactions, such as the oxidation of CO over transition metal catalysts and the synthesis of ammonia over iron- and ruthenium-based catalysts, the pressure and the materials gaps have been successfully bridged [3]. Under these favorable conditions the gained knowledge on the molecular level may in turn push the search for improved catalysts towards rational design.

Peden and Goodman [4] reported on an apparent pressure gap for the oxidation of CO over the Ru(0001) surface. While under UHV conditions ruthenium is by far the poorest catalyst for CO oxidation among the late transitions metals due to the very high binding energy of adsorbed atomic oxygen, this ranking in catalytic activity reverses, when CO oxidation proceeds under high pressure and oxidizing reaction conditions. Here, Ru turns out to be much more active than the other late transition metals. Fifteen years later this pressure gap puzzle has been partly (if not fully) disentangled. Under realistic CO oxidation reaction conditions the initially metallic Ru catalyst transforms into RuO_2, which turned out to be the catalytically active phase of the working catalyst [5]. It has to be noted that ruthenium exhibits outstanding catalytic properties. Promoted metallic ruthenium is known to be the best hydrogenation catalyst for dinitrogen and therefore the most active ammonia synthesis catalyst [6]. Correspondingly, ruthenium might be expected to be a poor oxidation catalyst. However, under oxidizing reaction conditions the Ru catalyst transforms into a very efficient oxidation catalyst in the form of RuO_2 [5].

The present review article summarizes our joint research effort of applied catalysis (Muhler and co-workers) and theoretical (Seitsonen) and experimental surface science (Over and co-workers) over the past six years. Our joint project has been devoted to bridge the pressure and materials gaps for the simple CO oxidation reaction over Ru-based catalysts (section 2). In section 3 we demonstrate how this knowledge gained in section 2 can be exploited to understand and to surmount the problem of structural deactivation of the RuO_2 catalysts under oxidizing reaction conditions. Section 4 focuses on the microscopic reaction steps in the catalytic CO oxidation over RuO_2(110). Experimental results together with DFT calculations are presented in sections 4.2–4.4 and critically compared to the existing literature. The results of a microkinetic analysis of catalytic data on RuO_2 powder catalysts obtained at atmospheric pressure are discussed in section 4.5 based on the surface science results. Section 5 concludes this review with a brief summary and a collection of potential applications of RuO_2 in the near future.

2. From model catalysts to applied catalysts: bridging the pressure and materials gaps

2.1. The preparation and characterization of Ru-based catalysts

In order to bridge the materials gap we prepared three different Ru-based catalysts. The preparation of the oxide-supported Ru catalysts Ru/SiO_2 and Ru/MgO are discussed first. As a natural link to the model catalysts based on single-crystalline RuO_2(110) and RuO_2(100) films, we used polycrystalline RuO_2 powder catalysts. The preparation recipes and first characterization results of these catalysts are presented.

2.1.1. Supported Ru catalysts. The supported Ru catalysts Ru/MgO and Ru/SiO_2 were prepared by the molecular organic chemical vapor deposition (MOCVD) method. $Ru_3(CO)_{12}$ (Strem) was used as Ru precursor and deposited on the commercially available supports MgO (Alfa Aesar, purity of 99.9955%) as well as on SiO_2 (Aerosil 200, Degussa). Further details about the procedure are described in [7]. For elemental analysis the samples were dissolved in a sodium peroxide solution and the Ru content was measured by inductively coupled plasma optical emission spectroscopy (ICP-OES). Based on the amount of the precursor the metal loading of the catalyst was adjusted. Supported catalysts with about 3 wt% Ru were used for the spectroscopic and kinetic studies.

Table 1. Characterization of the supported Ru/MgO and Ru/SiO_2 catalyst based on elemental analysis and H_2 chemisorption.

Supported catalyst	Metal surface ($m^2\ g^{-1}$)	Metal content (%)	Dispersion (%)	Average crystallite size (nm)
Ru/MgO	9.9	3.21	63.4	1.6
Ru/SiO_2	10.2	3.02	68.5	1.5

The particle size of the supported Ru particles was investigated by H_2 chemisorption measurements and by transmission electron microscopy (TEM). H_2 chemisorption was primarily used to determine the specific metal surface area and the dispersion, but also offers the possibility to estimate the Ru particle size. The experiments were carried out at 298 K after a reductive pretreatment up to 773 K [8]. Results based on extrapolating the hydrogen pressure to zero, a surface stoichiometry of $H_{ads}/Ru_{surf} = 1$, a metal density of 12.3 g cm^{-3}, and an average area of 8.17 $Å^2$ per Ru atom are summarized in table 1. A high Ru dispersion of 63% and 69% is found for Ru/MgO and Ru/SiO_2 catalysts respectively; Ru dispersion is defined as the ratio of exposed Ru surface atoms to the total number of Ru atoms. Obviously, the preparation method is widely independent of the support material. The calculated average crystallite size is about 1.5 nm assuming spherical particles.

TEM micrographs of Ru/MgO and Ru/SiO_2 catalysts confirmed the small size of the supported Ru particles. In the case of Ru/SiO_2 a mean particle size of 2.5 nm was determined from the particle size distribution. For the system Ru/MgO, a Ru particle size of 1 nm or less was estimated from the size distribution [8].

2.1.2. Polycrystalline RuO_2 powder catalysts. Polycrystalline RuO_2 powder (purity > 99.9%, supplied by Merck Ltd) was chosen for detailed investigations. Due to the particle size of about 0.5 μm determined by x-ray diffraction (XRD) [9], RuO_2 powder catalysts can be considered as a natural link between the supported Ru nanoparticles and the model single-crystal surfaces (cf section 2.1.3). Reduction of the polycrystalline RuO_2 powder at 773 K using hydrogen is sufficient to form microscale Ru metal powder as indicated by XRD. The surface area measured by BET (RuO_2 and Ru powder) as well as by H_2 chemisorption (Ru metal powder) was not strongly affected by the reduction process and amounts to 1.3 $m^2\ g^{-1}$ [9].

Polycrystalline nanoscale RuO_2 (purity > 99.99%, supplied by Alfa Aesar) was investigated in order to understand the dependence of catalytic activity and stability on the particle size. The BET surface area of the as received RuO_2 powder amounts to 79.0 $m^2\ g^{-1}$, and the metal surface area after hydrogen reduction at 773 K amounts to 16.0 $m^2\ g^{-1}$. By different inert gas and oxidative treatment it is possible to stabilize the BET surface area at 7.2 $m^2\ g^{-1}$.

2.1.3. RuO_2 model catalysts: RuO_2(110) and RuO_2(100) films. The RuO_2(110) film on a well-prepared Ru(0001) surface was produced by an O_2 exposure of 3×10^6 L (one langmuir: 1 L corresponds to a dose of 1.3×10^{-6} mbar s) in ultrahigh vacuum (UHV) environment. The preparation temperature was in the range of 550–650 K [10]. Above 700 K the prepared RuO_2(110) becomes significantly roughened. The dimensions of the surface (1×1) unit cell of RuO_2(110) are 3.12 Å × 6.38 Å [11]. In order not to break the UHV conditions we applied for these high O_2 exposures a microcapillary arrays shower. This allowed us to keep the pressure in the UHV chamber below 10^{-5} mbar while the pressure at the sample surface was about 10^{-3}–10^{-2} mbar.

The RuO_2(100) film was produced by excessive exposure of a well-prepared Ru(10$\bar{1}$0) surface to molecular oxygen (circa 3×10^5 L O_2), keeping the sample temperature at 600–700 K. The dimensions of the surface (1×1) unit cell of RuO_2(100) are 3.12 Å × 4.28 Å [12]. The LEED pattern exhibits a c(2×2) symmetry. CO adsorption experiments demonstrate that the c(2×2) LEED pattern consists actually of (1×1) domains in coexistence with c(2×2) domains [12].

The active catalyst surface is in both cases about 1 $cm^2\ g^{-1}$, i.e. by 4–6 orders of magnitude smaller than powder or supported catalysts.

2.2. Complex Ru–O chemistry

2.2.1. Oxygen chemistry of single-crystalline Ru surfaces. When exposing the Ru(0001) surface to molecular oxygen under UHV conditions, a (2×2)-O and a (2×1)-O overlayer is formed [13]. The dissociative sticking coefficient drops from almost one to less than 10^{-3}, so that under normal UHV conditions the (2×1)-O phase was considered as the saturation phase. Dosing much more oxygen, say more than 10^3–10^6 L at room temperature the Ru(0001) surface stabilizes two additional phases of chemisorbed oxygen, namely the (2×2)-3O [14] and the (1×1)-O [15]. The dissociative sticking coefficient of oxygen over the Ru(0001)-(1×1)-O surface is estimated to be less than 10^{-6} [16]. Consequently, oxygen uptake beyond a coverage of 1ML becomes the rate determining step for the initial oxidation of Ru(0001). However, as soon as an oxide nucleus is formed on the Ru(0001)–(1×1)O surface, the progressing oxide formation proceeds in an autocatalytic way [17], since the sticking coefficient on the oxide surface is as high as 0.7 [16]. Autocatalytic oxidation means that the surface produces its own 'catalyst' in the form of small oxide nuclei to efficiently dissociate the oxygen molecules, resulting in a self-acceleration of the oxidation process. The identification of autocatalytic oxidation kinetics is supported by scanning tunneling microscopy (STM) measurements [20] and scanning photoemission microscopy (SPEM) images [18], which show that the homogeneous Ru(0001) becomes partly heterogeneous upon oxidation due to the coexistence of (1×1)-O and RuO_2(110) patches on the surface, both of which are several microns wide. Obviously, as soon as an oxide nucleus is formed, it grows rapidly across the surface. The threshold temperature for oxidation of Ru(0001) with molecular oxygen turns out to be 540 K. Below this temperature RuO_2(110) cannot be formed on Ru(0001) for $P(O_2) < 10^{-1}$ mbar [11]. Instead, on the basis of high pressure XPS (HP-XPS) experiments a non-stoichiometric

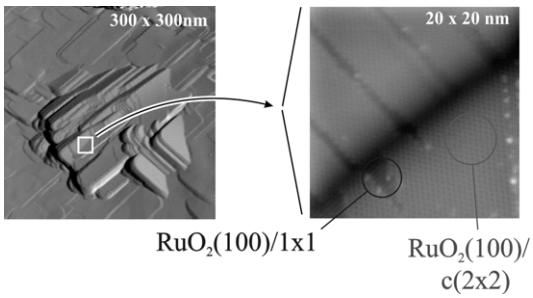

Figure 1. The initial roughening of a $RuO_2(110)$ film on Ru(0001). Left: STM image (300 nm × 300 nm). Right: zooming into the rough region (STM image: 20 nm × 20 nm) indicates that the facets are oriented along the (100) direction and reconstructed into a c(2 × 2) phase. The figure is adopted from [22].

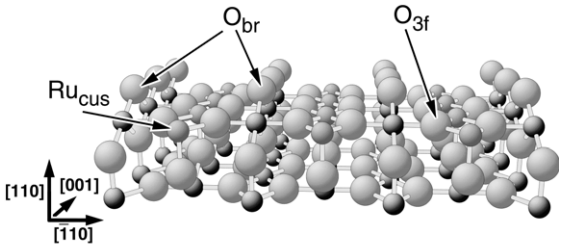

Figure 2. Ball and stick model of the clean $RuO_2(110)$ surface. Large balls represent oxygen, and small balls represent ruthenium atoms of $RuO_2(110)$. The bridge-bonded oxygen atoms O_{br} and cus Ru atoms are indicated. Both surface species are onefold undercoordinated with respect to the bulk coordination, representing the active catalytic sites of the $RuO_2(110)$ model catalyst.

transient surface oxide (TSO) has been proposed to form in the temperature range from 400 to 500 K [19]. Below 400 K, only chemisorbed oxygen can be stabilized on Ru(0001).

In situ surface x-ray diffraction (SXRD) measurements [11] are fully consistent with the proposed autocatalytic oxidation process of Ru(0001). The produced $RuO_2(110)$ film on Ru(0001) is 1.6 nm thick over a wide temperature (580–630 K) and pressure range (10^{-5}–10^{-1} mbar) [11]. This means that there is a self-limited growth of $RuO_2(110)$ on Ru(0001). Above 670 K the RuO_2 film is able to grow thicker, but at the expense that the Ru/RuO_2 surface/interface roughens substantially forming various facets and transforming the surface into a catalytically inactive RuO_2 oxide [12, 21]. The initial roughening of the RuO_2 film is illustrated by STM images shown in figure 1.

In the bulk structure of RuO_2 (rutile structure) the ruthenium atoms bind to six oxygen atoms, forming a slightly distorted RuO_6 octahedron, while the oxygen atoms are coordinated to three Ru atoms in a planar configuration that is consistent with an sp^2 hybridization of oxygen. The dimensions of the $RuO_2(110)$ surface unit cell are 3.12 Å × 6.38 Å [11], which is incommensurate to the Ru(0001) surface.

On the stoichiometric $RuO_2(110)$ surface (cf the ball and stick model of the bulk-truncated $RuO_2(110)$ surface shown in figure 2) two kinds of undercoordinated surface atoms are present and organized in rows along the [001] direction: (i) the

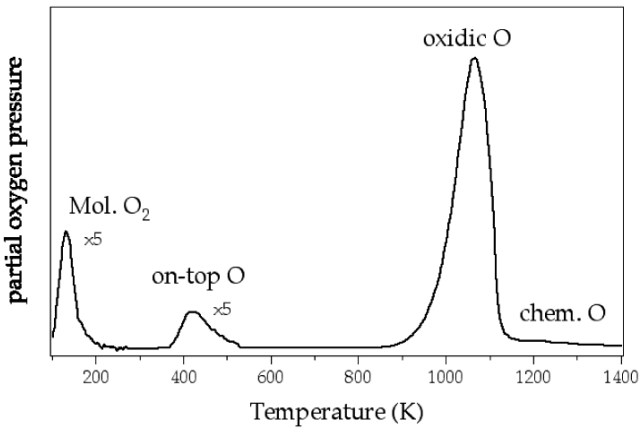

Figure 3. Thermal desorption spectra of oxygen on Ru(0001) and $RuO_2(110)$ [26]. The desorption states chem. O, oxidic O, on-top O and mol. O_2 correspond to chemisorbed oxygen on Ru(0001), lattice oxygen of $RuO_2(110)$, weakly held on-top oxygen on $RuO_2(110)$, and molecular oxygen on $RuO_2(110)$. The spectrum of Mol. O_2 and on-top O is amplified by a factor of 5.

bridging oxygen atoms O_{br}, which are coordinated only to two Ru atoms underneath (instead of three) and (ii) the so-called cus Ru atoms (*cus* stands for coordinatively unsaturated sites) [20]. Both undercoordinated surface atoms (cus Ru and O_{br}) can clearly be resolved with core level spectroscopy [23] and with STM [24]. These types of undercoordinated surface atoms are equally present on $RuO_2(100)$ and $RuO_2(101)$ [25].

Oxygen exposure of the stoichiometric $RuO_2(110)$ surface at room temperature leads to the population of the atomic oxygen adsorbed on top of the cus Ru atoms (cf on-top O in figure 3). Exposure of 5 L of O_2 saturates most of the cus Ru atoms by on-top O atoms (O_{ot}). Oxygen exposure at 100 K stabilizes also a molecular oxygen species on the $RuO_2(110)$ surface. When annealing the $RuO_2(110)$ surface beyond 900 K, the oxide decomposes with a maximum oxygen desorption at 1050 K. The residual oxygen which is left on the surface beyond 1050 K is attributed to chemisorbed oxygen on Ru(0001).

The orientation of the RuO_2 film depends on the orientation of the underlying Ru substrate. For instance, on Ru(0001) RuO_2 grows preferentially in (110) orientation [10], while on Ru(10$\bar{1}$0) RuO_2 grows in (100) orientation [12]. In figure 4 we show a typical STM image of the $RuO_2(100)$ surface together with a ball and stick model of the $RuO_2(100)$-(1 × 1) surface. The $RuO_2(100)$-(1 × 1) surface exposes bridging O atoms and cus Ru atoms similar to the $RuO_2(110)$ surface, that is, the main structural elements are preserved. The (1 × 1) phase of $RuO_2(100)$ is catalytically active in the oxidation of CO, while the c(2 × 2) phase of $RuO_2(100)$ is inactive in the CO oxidation. This finding will be of importance for the explanation of the structural deactivation of polycrystalline powder catalysts under oxidizing reaction conditions. Recent *in situ* HP-XPS studies have demonstrated that the threshold temperature for the formation of $RuO_2(100)$ of Ru(10$\bar{1}$0) is 450 K [19]. In the temperature range from 400 to 450 K only a transient surface oxide (TSO) is stabilized on the Ru(10$\bar{1}$0) surface.

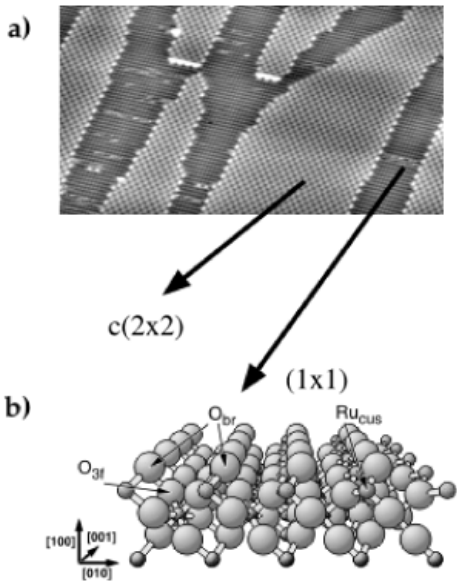

Figure 4. (a) Experimental STM image (constant current mode, taken at room temperature) of the $RuO_2(100)$ surface: 12 nm × 30 nm, $U = -0.80$ V, $I = 0.59$ nA. (b) Ball and stick model of the stoichiometric $RuO_2(100)$-(1 × 1) surface. Bulk O and Ru atoms are shown as large and small balls, respectively. A bridge-bonded O (O_{br}) and a undercoordinated Ru atom Ru_{cus} are indicated [27].

A threshold temperature of 450 K is also found for 2–6 nm thick nanocrystalline Ru films supported on Si(001) [31]. Obviously, the oxidation of ruthenium needs a minimum threshold temperature to occur. In table 2 the experimentally found values for the oxidation threshold temperatures are compiled.

2.2.2. Oxygen chemistry of polycrystalline Ru powder catalysts. The low energy crystal planes of RuO_2 are the (110), (100) and (101) orientations. From DFT calculations the surface energies of $RuO_2(110)$, $RuO_2(100)$ and $RuO_2(101)$ were determined to be 71 meV Å^{-2}, 87 meV Å^{-2} and 76 meV Å^{-2}, respectively [28]. Therefore, the (110) orientation is expected to be the most abundant orientation of polycrystalline RuO_2. All the bulk-truncated surfaces of low energy orientations of RuO_2 expose cus Ru sites and

Table 2. Compilation of the threshold temperatures for the surface oxidation of various Ru single crystals exposed to molecular oxygen.

Catalyst system	Threshold temperature for full oxidation (K)
Ultrathin $RuO_2(110)$ on Ru(0001)	540 [11]
TSO on Ru(0001)	400–530 [19]
Ultrathin $RuO_2(100)$ on Ru(10$\bar{1}$0)	450 [19]
TSO on Ru(10$\bar{1}$0)	400–450 [19]

bridging O atoms. Consequently, we do not expect to observe a pronounced structure sensitivity of the CO oxidation reaction on RuO_2 [25]. Scanning electron microscopy (SEM) in combination with electron back scattering diffraction (EBSD) of polycrystalline RuO_2 indicates that the (110) orientation is indeed prevailing (cf figure 5).

Supported Ru nanoparticles on MgO or SiO_2 with dimensions of 2–3 nm readily oxidize under reaction conditions even at room temperature [8, 30]. The integral stoichiometry of these oxidized Ru particles was determined to be $RuO_{1.5}$. Since Ru can only form RuO_2 as the stable solid oxide, a Ru:O stoichiometry of 1.5 points to a shell–core particle [8, 30]: the shell consists of an ultrathin RuO_2 film coating the metallic Ru core. The exposure to flowing oxygen at 470 K resulted in the full oxidation of the supported RuO_2/Ru nanoparticles [30]. For the bulk oxidation of microscale RuO_2/Ru shell–core particles in flowing oxygen, temperatures above 573 K were found to be necessary [9, 35] in agreement with the onset of RuO_2 film thickening on Ru(0001) (cf section 2.2.1).

The temperature-programmed O_2 desorption experiments (TPD) were carried out with 134.5 mg of nanoscale RuO_2 powder (*Alfa Aesar*, BET surface area of 79 m^2 g^{-1}). The fresh nanoscale powder catalyst was heated in He to 523 K applying a heating ramp of 5 K min^{-1} and then held for 1 h at this temperature to remove adsorbed hydrocarbons and water. After cooling down to 423 K in He, the flow was changed to 100% O_2 and the temperature was held for 30 min. During the following 30 min the catalyst was cooled down to 398 K and then during further 30 min to room temperature. At room temperature the catalyst was flushed in He for 30 min. This treatment is supposed to assure complete coverage of on-top O on the cus Ru sites. The TPD of O_2 in He was carried out applying heating rates of 3 K min^{-1}, 5 K min^{-1}, and 7 K min^{-1}, respectively

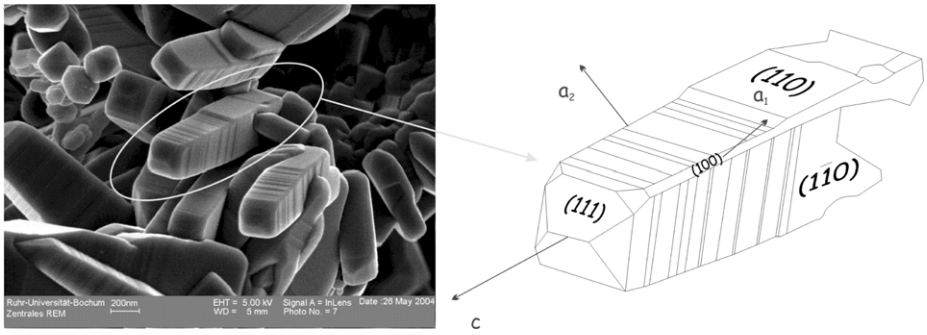

Figure 5. SEM micrograph of polycrystalline RuO_2. The typical size of the RuO_2 columns is 300 nm × 300 nm in width and several microns in length. The orientations of the facets (left side) were determined by using electron back scattering diffraction [9, 29].

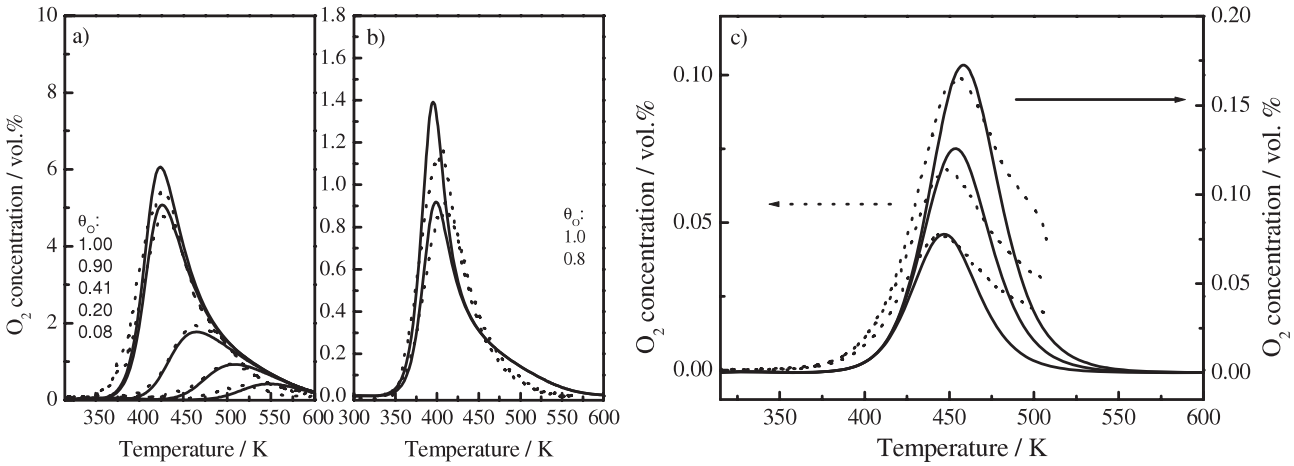

Figure 6. Single-crystal O_2 TPD studies (dotted lines) [16] (a) and [34] (b), and simulated curves (solid lines) based on the coverage-dependent model for UHV conditions ($p = 10^{-10}$ mbar, a) $\beta = 360$ K min^{-1}, (b) $\beta = 60$ K min^{-1}. (c) Oxygen concentrations (dotted lines) as a function of temperature detected during temperature-programmed desorption from nanoscale RuO_2, applying heating rates of 3, 5, and 7 K min^{-1}. These experiments are compared to the coverage-independent second-order model (solid lines).

(cf figure 6(c)). The final temperature of the TPD experiments was set to 500 K, which was held for 45 min.

Assuming an exposed surface of 20×10^{-20} m^2 per unit cell of $RuO_2(110)$, one cus Ru site per unit cell [11], and taking the BET area of 79 m^2 g^{-1} area into account, a total oxygen coverage of 0.7 ML is calculated. This value is close to the saturation coverage of 0.8 ML obtained on $RuO_2(110)$ [26].

The experimental TPD profiles in figure 6(c) have the typical shape of second-order desorption kinetics, with the peak maxima shifting to higher temperatures with increasing heating rate [32]. Differences from the ideal behavior are the long tailing and the slight shift of the onset of desorption. The temperatures of the peak maxima are in fairly good agreement with corresponding experiments on the $RuO_2(110)$ model catalyst (cf figure 3) allowing us to identify the desorbing oxygen species with the on-top O species. The desorption energy and the pre-exponential factor were derived by an improved heating rate variation method according to Falconer and Schwarz [32] and the Redhead method [33]. The resulting kinetic parameters are $E_{\mathrm{des}} = 117 \pm 7$ kJ mol^{-1} and $A_{\mathrm{des}} = 2.6 \times 10^{11}$ s^{-1}. With the same method we determined an activation energy of 117 ± 7 kJ/mol and $A_{\mathrm{des}} = 8.9 \times 10^{13}$ s^{-1} for the case of single-crystalline $RuO_2(110)$. As the desorption of O_2 occurs in a fixed-bed reactor, readsorption on empty sites can occur leading to broad TPD peaks shifted to higher temperatures. The narrow widths of the TPD profiles shown in figure 6(c) clearly demonstrate the absence of readsorption for the atmospheric pressure experiments. Thus, the adsorption of O_2 must be a kinetically hindered process due to the high coverage of on-top O [35]. It is reasonable to explain the kinetically hindered adsorption of O_2 at higher coverages by the high diffusion barrier of on-top O along the cus Ru rows which inhibits the creation of two neighboring free cus Ru sites for the dissociation of molecular oxygen (cf section 4.4).

A simple microkinetic model based on second-order desorption kinetics and the derived values from the heating rate variation is able to reproduce the desorption temperatures of the experiments using the mass balance of a continuously stirred tank reactor (CSTR):

$$\frac{c_{\mathrm{O_2}} - c_{\mathrm{O_2},0}}{\tau} = A_{\mathrm{des}} \exp\left(\frac{-E_{\mathrm{des}}}{RT}\right) \times \theta_{\mathrm{O}}^2 - A_{\mathrm{ads}} \exp\left(\frac{-E_{\mathrm{ads}}}{RT}\right) p_{\mathrm{O_2}} (1 - \theta_{\mathrm{O}})^2,$$

where τ is the residence time. By insertion of the derived values of $E_{\mathrm{des}} = 117 \pm 7$ kJ mol^{-1} and $A_{\mathrm{des}} = 2.6 \times 10^{11}$ s^{-1}, and under the assumption that readsorption does not occur, that is, $k_{\mathrm{ads}} = 0$, the experimental data shown in figure 6(c) can be reproduced by this simple second-order model without parameter fitting.

This simple model is not able to reproduce the pronounced tailing of the TPD peaks at higher temperatures. Therefore, the desorption energy was modified using a coverage-dependent activation energy of desorption $E_{\mathrm{des}} = 117 + 28(1 - \theta_{\mathrm{O}})^{3.2}$ kJ mol^{-1}, which is in good agreement with very recent DFT calculations [36]. Also the TDS profiles obtained with single crystals [16, 34] for various initial oxygen coverages can be reproduced by this refined model (figures 6(a) and (b)). Therefore, according to the O_2 TPD experiments the pressure and the materials gaps are bridged for the interaction of O_2 with RuO_2.

2.3. The stability of RuO_2 under reducing reaction conditions using an excess of CO

2.3.1. The reduction of $RuO_2(110)$ by CO. Carbon monoxide (CO) is an efficient reducing agent of the $RuO_2(110)$ surface [37] when no additional oxygen is supplied. CO exposure around room temperature already replaces all bridging oxygen atoms from the stoichiometric $RuO_2(110)$ surface by bridging CO molecules [37]. This surface is referred to as mildly reduced $RuO_2(110)$ surface, since essentially no morphological modifications occur on the oxide surface. At temperatures below and around room temperature CO also

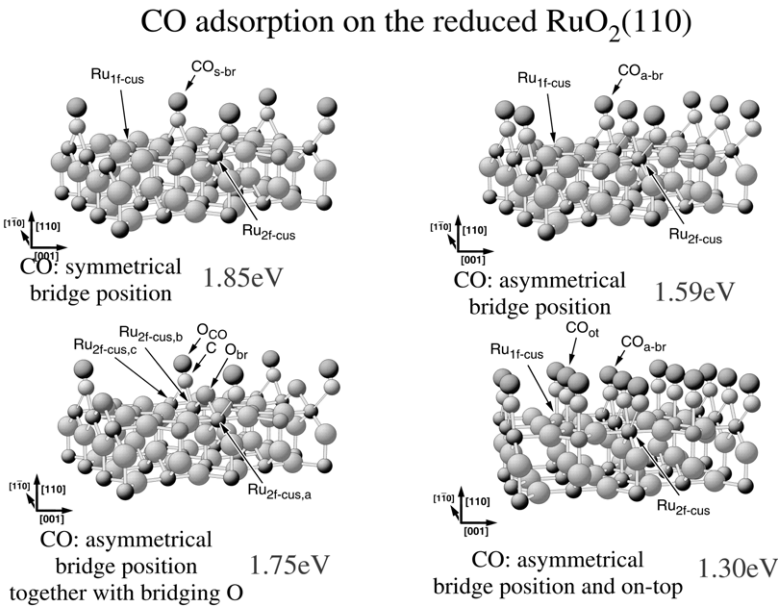

Figure 7. Variety of CO adsorption sites are possible on the mildly reduced $RuO_2(110)$ surface. The energetically most favored CO adsorption site is the symmetric bridging site (1.85 eV), followed by the asymmetric bridging position (1.59 eV). For this adsorption case all bridging oxygen atoms O_{br} are replaced by CO, while for the symmetric bridging CO only every second bridging Ru atoms is occupied. Around and below room temperature also the cus Ru atoms are occupied by CO. The adsorption energy of on-top CO decreases, however, to 130 kJ mol^{-1} [37].

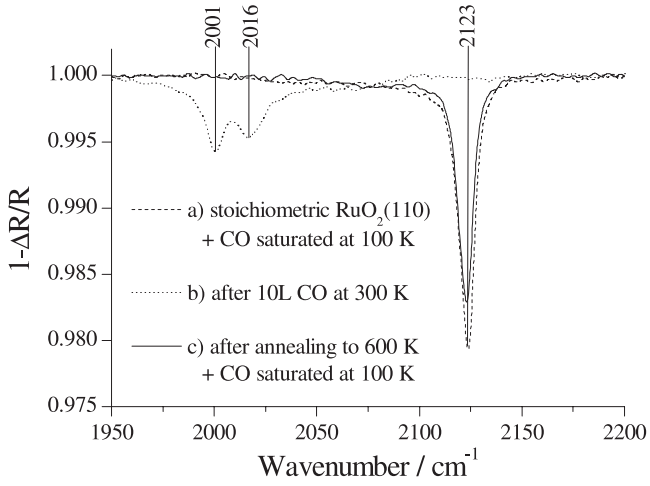

Figure 8. CO RAIRS experiments are performed for (a) the stoichiometric $RuO_2(110)$ surface saturated by CO at 100 K, (b) the mildly reduced $RuO_2(110)$ surface by exposing 10 L of CO at room temperature, (c) and annealing the mildly reduced surface to 600 K. These RAIRS experiments disclose the chemical nature of the $RuO_2(110)$ surface. For the stoichiometric and the annealed surface, CO post adsorption at 100 K was used for probing the chemical state of the surface. The RAIRS experiments are unpublished [38].

occupies the cus Ru atoms, resulting in a variety of surface structures which are summarized in figure 7.

In figure 8 reflection absorption infrared spectroscopy (RAIRS) experiments are presented for the initial reduction of $RuO_2(110)$ by CO exposure. RAIRS allows to determine the chemical nature of the topmost $RuO_2(110)$ surface by using CO as a probe molecule. CO adsorption at 100 K on the stoichiometric $RuO_2(110)$ surface discloses only one vibration frequency at 2123 cm^{-1}, which is assigned to on-top CO on the stoichiometric $RuO_2(110)$ surface. When the stoichiometric $RuO_2(110)$ surface is exposed to 10 L of CO at 300 K, then two vibrational features appear, which are assigned to bridging CO (2001 cm^{-1}) and on-top CO (2016 cm^{-1}). Annealing this mildly reduced surface to 600 K and subsequently saturating the surface with CO at 100 K leads to a RAIRS spectrum which is practically identical to that of the stoichiometric $RuO_2(110)$ surface, indicating that most of the mildly reduced $RuO_2(110)$ surface has been restored to the stoichiometric $RuO_2(110)$ surface. According to recent STM investigations [27] the required oxygen is originating from the oxide producing holes in the $RuO_2(110)$ oxide. The excess Ru agglomerates into small islands at the rim of the holes. The mildly reduced $RuO_2(110)$ surface separates after annealing to 600 K into a restored stoichiometric $RuO_2(110)$ with holes and small Ru clusters. This behavior reflects nicely the fact that only a single solid Ru oxide exists, namely RuO_2.

For *in situ* reduction experiments we applied the technique of surface x-ray diffraction (SXRD) [11]. We exposed first a 1.6 nm thick $RuO_2(110)$ film on Ru(0001) to $p(CO) = 10^{-5}$ mbar, keeping the sample temperature at 418 K. The progressing reduction of RuO_2 by CO was monitored *in situ* by the evolution of the integral x-ray intensities of a RuO_2-related SXRD reflection (cf figure 9). For a sample temperature of 370 K no severe reduction of $RuO_2(110)$ is observed, while at a sample temperature of 415 K the SXRD intensity decreases linearly with exposure time. No induction period occurred within the experimental time resolution of 100 s.

2.3.2. The reduction of polycrystalline powder catalysts by CO. The interaction of CO with the oxidized Ru/MgO

Table 3. Observed CO stretching vibrations in cm^{-1} determined by *in situ* DRIFTS for the oxidized supported catalysts $Ru/MgO(SiO_2)$ and *in situ* RAIRS and HREELS for the model catalyst $RuO_2(110)$. The assignment of these experimentally found vibrations to particular CO species on the oxide surface is based on density functional theory (DFT) calculations and structural analysis using low energy electron diffraction (LEED).

$Ru/MgO(SiO_2)$ *in situ* DRIFTS [8] $p(CO) = 100$ mbar	$RuO_2(110)$ *in situ* RAIRS [38] $p(CO) = 10^{-8} \ldots 10^{-2}$ mbar	$RuO_2(110)$ HREELS [39] *ex situ* $p(CO) = 10^{-8}$ mbar	$RuO_2(110)$ DFT [37]	$RuO_2(110)$ LEED [37]
2125 (2130)	2110–2120	2115	2085	On top
1995 (2016)	1995/1898	1975/1895	1994/1897	Asym./sym. bridge
2072 (2074)	2073	2072	—	Asym. + ontop coupled

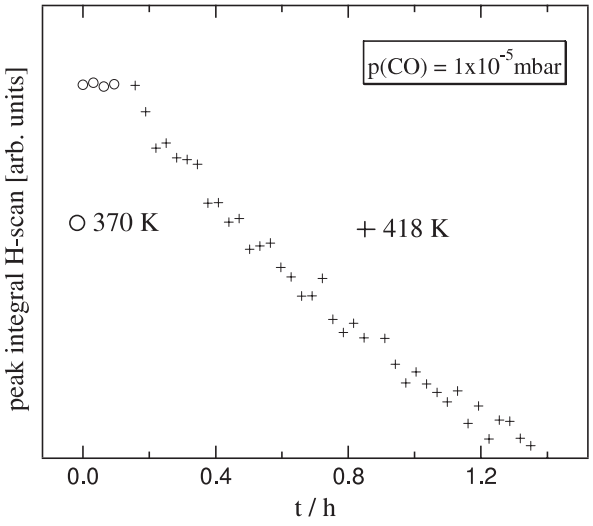

Figure 9. Reduction of a 5 ML thick $RuO_2(110)$ film on Ru(0001) by exposure to 10^{-5} mbar of CO at a sample temperature of 418 K. The integral intensities of a RuO_2 related reflection (at 0.733 along the **H** direction) are depicted as a function of CO exposure time.

and Ru/SiO_2 catalysts was intensively studied by *in situ* diffuse reflectance infrared Fourier transform spectroscopy (DRIFTS) [8]. Oxidation of the supported Ru catalysts was performed at 308 K for 2 h in a continuous 10% O_2/Ne feed and purging in argon for 15 min, followed by the exposure to CO in a continuous flow of a 10% CO/Ne mixture at 308 K. The corresponding *in situ* DRIFTS spectra in the CO stretching vibration region are compiled in figure 10 for various CO exposures, keeping the CO partial pressure constant and recording successively DRIFT spectra.

At the beginning of the adsorption process, two bands can be observed at 2125 (2130) and 2072 (2074) cm^{-1} for Ru/MgO (Ru/SiO_2). Gaseous CO_2 and gaseous CO were detected, too. A new band arose at about 1995 cm^{-1} in case of Ru/MgO and at 2016 cm^{-1} for Ru/SiO_2. Both the appearance of this new band and the formation of gaseous CO_2 during the CO treatment indicate that the oxidation of CO is associated with a mild reduction of the RuO_2 surface. A full reduction of RuO_2 to Ru is not possible at room temperature consistent with corresponding *in situ* RAIRS experiments of the model catalyst $RuO_2(110)$. The assignments of the various CO bands to particular CO species are based on DFT and LEED results and the experimental findings for supported catalysts (DRIFTS) and model catalyst (RAIRS, HREELS) are summarized in table 3. The agreement of the vibrational data of the supported catalysts and those obtained for the model catalyst is intriguing, as both the materials and the applied pressures are very different. This comparison indicates impressively that both the pressure and materials gap have successfully been bridged spectroscopically.

The stability of the unsupported RuO_2 catalyst was investigated by temperature-programmed reduction (TPR) experiments using CO as the reducing agent. According to the experiments shown in figure 11, the RuO_2 powder catalyst is fully reduced at 560 K, a temperature that is significantly higher than that found for 1.6 nm thick $RuO_2(110)$ supported on Ru(0001) (about 400 K). Just for comparison, also TPR experiments applying H_2 as the reducing agent are shown.

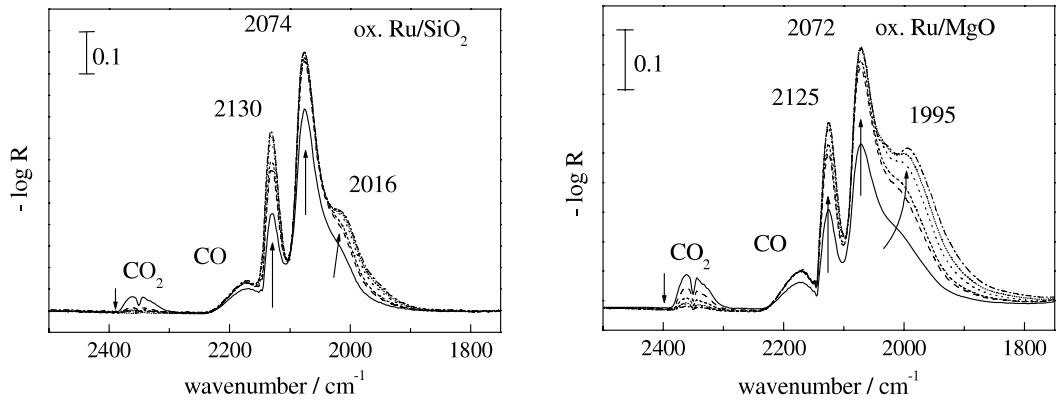

Figure 10. DRIFT spectra of oxidized Ru/MgO (left side) and Ru/SiO_2 (right side) for various CO exposures at room temperature. 10% CO/Ne flow at atmospheric pressure and $T = 308$ K. Spectra were recorded after 1 min (solid line), 2 min (long dashes), 10 min (dotted), 20 min (short dotted) and 30 min (dash–dotted) exposure to CO [8].

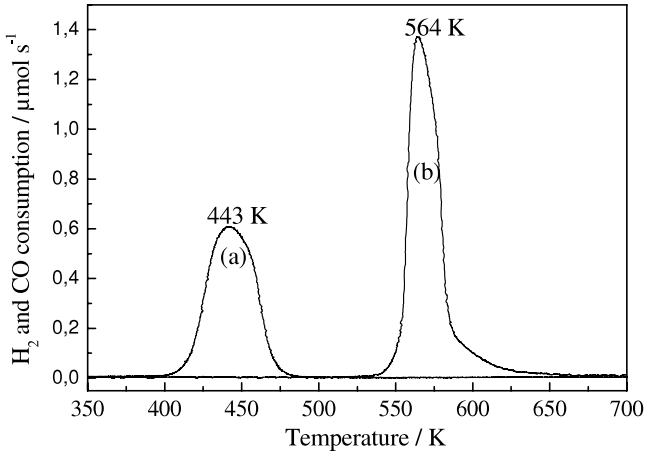

Figure 11. TPR profiles of polycrystalline RuO_2 using different reducing agents: (a) H_2, and (b) CO. Heating ramp: 10 K min^{-1} [9].

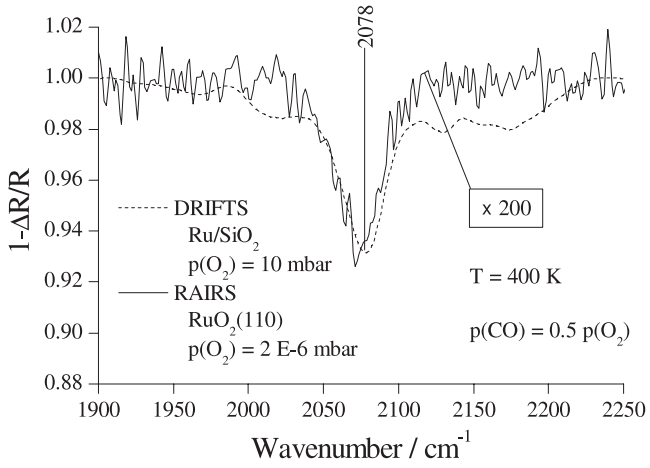

Figure 12. *In situ* infrared spectra during the CO oxidation reaction over supported RuO_2/SiO_2 catalyst (DRIFTS [8]) in comparison with that over the model catalyst $RuO_2(110)$ (RAIRS [38]).
$p(CO) = 0.5p(O_2) = 10$ mbar for the RuO_2/SiO_2 studies.
$p(CO) = 0.5p(O_2) = 2 \times 10^{-6}$ mbar for the RuO_2/SiO_2 studies.

Here, the RuO_2 powder catalyst can already be reduced at 443 K, fully consistent with corresponding studies for the model catalyst $RuO_2(110)$ (415 K) [11].

2.4. The successful bridging of the pressure and materials gaps for the catalytic CO oxidation over RuO_2: spectroscopic and kinetic evidences

The first attempt to bridge the pressure and materials gap under reaction conditions is based on FTIR spectroscopy. Here, we compare the *in situ* infrared spectrum of supported RuO_2 catalyst with that of the $RuO_2(110)$ model catalyst, applying the techniques of DRIFTS and RAIRS, respectively. Although the partial pressures are very different, that is 10 mbar versus 2×10^{-6} mbar for the supported RuO_2 catalyst and the model catalyst $RuO_2(110)$, respectively, the dominant CO vibrational feature in both cases (figure 12) is the band at 2078 cm^{-1}. This CO stretch vibration is assigned to CO in densely packed CO domains comprising of bridging and on-top CO (cf figure 7). This finding indicates that from a spectroscopic point of view both the materials and the pressure gap are successfully bridged.

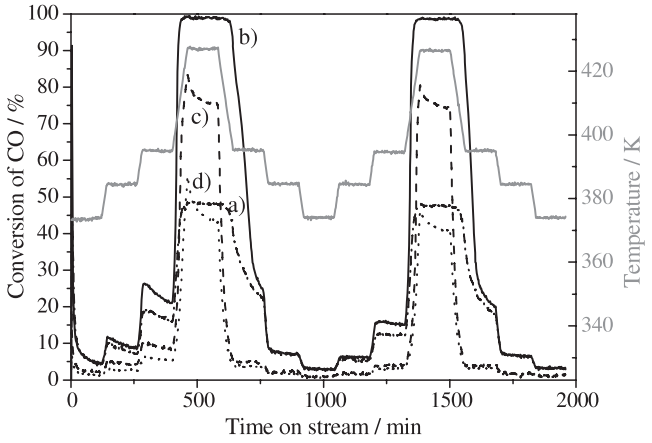

Figure 13. Conversion of CO over 12.5 mg of Ru/MgO diluted with 75 mg quartz as a function of time and temperature. The temperature program is displayed by the gray trace. The total flow rate was 50 ml(STP) min^{-1} with a CO/O_2 reactant feed ratio of (a) 4 (dash–dotted line), (b) 2 (full line), (c) 1 (dashed line) and (d) 0.5 (dotted line).

For bridging the pressure gap kinetically catalytic activity measurements were performed at atmospheric pressure and under vacuum conditions using the temporal analysis of products (TAP) reactor. The performance of temperature-programmed and isothermal experiments in the vacuum-flow mode of the TAP reactor allows us to measure the catalytic activity without facing mass transfer limitations or hot spots. The mean volumetric flow rate calculated from the pressure drop in the gas container amounts to only about 1 ml min^{-1} [8]. Full conversion of CO and O_2 for the CO oxidation over Ru/SiO_2 is achieved in the TAP reactor using a stoichiometric CO/O_2 ratio of 2. Due to full conversion of CO even down to temperatures of 353 K, the numbers of CO_2 molecules produced per metal surface site per second (turnover frequency, TOF) were only calculated for steady-state values obtained at 334 and 316 K and compiled in figure 14.

In contrast to TAP experiments, measurements at atmospheric pressure using a fixed-bed microreactor under plug–flow conditions (total flow in the range of 50–150 ml (STP) min^{-1}) were influenced by the highly exothermic heterogeneous oxidation reaction especially at high degrees of conversion. The catalytic activity measurements at atmospheric pressure were conducted at temperatures in the range of 298–423 K for different CO/O_2 reactant feed ratios (see figure 13). Before starting the oxidation of CO the supported catalysts Ru/MgO and Ru/SiO_2 were reduced in a 5% hydrogen/inert gas mixture up to 773 K. Figure 13 shows the conversion of CO over Ru/MgO for various CO/O_2 ratios as a function of time on stream and temperature. The starting temperature was 373 K, which was increased stepwise to 423 K, and subsequently reduced to the initial temperature. This procedure was repeated in a second cycle. During the first heating ramp, a decrease in activity can be observed after

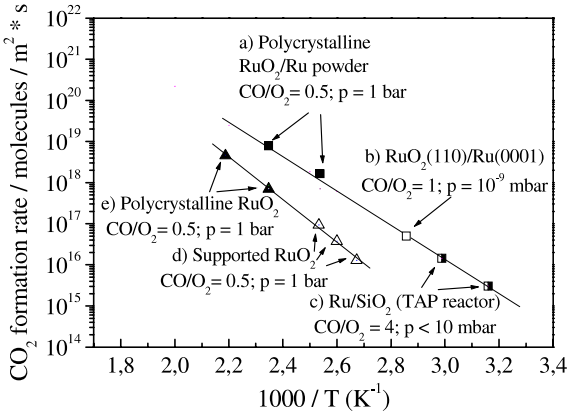

Figure 14. Arrhenius plot of rates of CO_2 formation [43] (TOF = turnover frequency, number of CO_2 molecules formed per active metal site per second) over the (d) Ru/SiO_2 catalyst for various CO/O_2 reactant feed ratios [8]. Also data are included that were obtained (a) with microscale polycrystalline RuO_2/Ru powder obtained by preceding reduction in H_2, (b) on a $RuO_2(110)$/Ru(0001) single crystal [40], (c) and (d) two silica-supported ruthenium catalysts prepared by impregnation [9], and (e) with microscale polycrystalline RuO_2 subsequent to heating in O_2 [9]. The activation energy derived from the upper Arrhenius line is 82 kJ mol^{-1}. From the lower line an activation energy of 86 kJ mol^{-1} is derived.

every increase in temperature for all experiments independent of the CO/O_2 reactant feed ratio. However, this deactivation process seems to be accelerated at higher O_2 pressures. In the second cycle, no further deactivation was observed during the heating ramp for the first two temperature steps, and the degrees of conversion of the following cooling steps are similar to those measured during the heating ramp in the first cycle. These observations imply that the deactivation is limited to the first temperature cycle.

To restore the high initial activity, the Ru/MgO catalyst had to be reduced in H_2 at 773 K. The observed deactivation was controlled by the reactant gas mixture and by the temperature. However, the ability to restore the initial high activity by chemical reduction indicates that sintering of the supported RuO_2/Ru nanoparticles is not the reason for the deactivation, a conclusion which was also confirmed by TEM measurements of the used samples [30].

Turnover frequencies were again derived for low degrees of CO conversion after steady state had been reached. These TOFs as well as TOFs calculated from the results obtained by the measurements under vacuum conditions in the TAP reactor are plotted in an Arrhenius diagram (cf figure 14). The TOF results show that an influence of the support on the activity can be neglected. There is very good agreement regarding the slope (activation energy of 82 kJ mol^{-1}) and the absolute scale. This activation energy is close to the value of 90 kJ mol^{-1} found in UHV studies of $RuO_2(110)$ [39]. The reaction rate for the oxidation of CO with a CO/O_2 reactant feed ratio of 2 at 321 K is of the order of about 10^{12} molecules cm^{-2} s^{-1}. Similar reaction rates were reported by Wang *et al* [40] for the steady-state oxidation of CO on a $RuO_2(110)$ single-crystal surface under UHV conditions.

These kinetic data show that the materials and pressure gap is successfully bridged for the upper Arrhenius line of figure 14. But figure 14 indicates also that there is a second lower Arrhenius line with a little higher activation energy of 86 kJ mol^{-1}, which is attributed to deactivation. It seems that on all investigated catalysts deactivation occurs, as further discussed in section 3.

The successful bridging of the pressure and materials gap under reaction condition is not too surprising, because in contrast to commonly used oxide surfaces the regular undercoordinated surface atoms (cus Ru and bridging O) of the stoichiometric $RuO_2(110)$ surface are the active centers, and not any highly active defect sites. In addition, we know that the efficiency for CO oxidation is not structure sensitive. This means that the efficiency for CO oxidation is almost independent of the orientation of RuO_2, at least for the (110), (100), and the (101) orientations, and is governed by the concentration of cus Ru atoms [25]. Since the (110), (100) and (101) surfaces of RuO_2 are low energy surfaces, these orientations are also the prevailing orientations on polycrystalline microscale and nanoscale RuO_2 particles.

3. Beyond the pressure and materials gaps

3.1. Structural deactivation of RuO_2 under reducing and oxidizing reaction conditions

In addition to activity and selectivity, catalyst deactivation during operation is a key issue in applied catalysis, because the frequent replacement of a catalyst results in high operational costs. For the Ru-based catalyst a strong activity loss was reported for the CO oxidation reaction. In particular under oxidizing reaction conditions the activity of supported Ru catalysts declines substantially [41, 42]. When we discussed the TOF over various Ru model catalysts (cf figure 14) and pressures in section 2, we recognized that there are two different Arrhenius lines, one for the active state and one for the deactivated state. The latter appears preferentially under oxidizing reaction reactions. The deactivation of the supported ruthenium catalysts during the oxidation of CO was observed at atmospheric pressures as well as under high vacuum conditions. Cant *et al* [41] concluded that portions of the metallic ruthenium surface are converted into an inactive oxide layer, whereas Kiss and Gonzalez [42] suggested that the partial deactivation of Ru/SiO_2 is the result of the formation of lattice oxygen. Both suggestions are not correct as shown in the following.

In figure 15 we present the CO conversion over a supported Ru/SiO_2 catalyst (mean particle size 2 nm) as a function of time on stream (CO/O_2 ratio of 2:1 at atmospheric pressures) at 400 K. Starting with a CO conversion of nearly 100% the conversion declined to about 20% during 15 h on stream, and steady-state conditions were still not yet reached. Similar deactivation behavior was observed for even stronger oxidizing reaction conditions [30]. During the first 5 h on stream there were pronounced oscillations in the CO conversion, which may be related to structural instabilities as discussed with the catalytic CO oxidation over

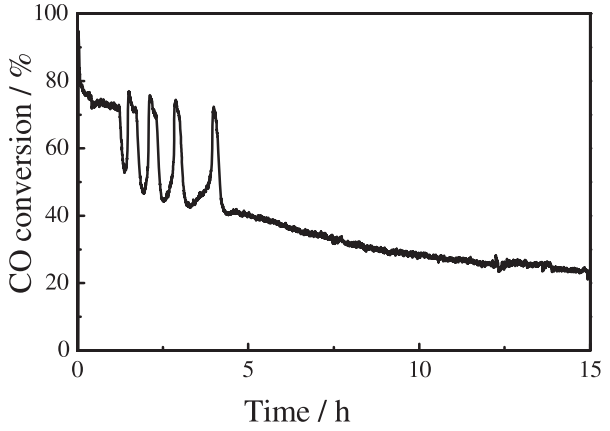

Figure 15. Conversion of CO for the oxidation of CO over 12.5 mg of Ru/SiO_2 diluted in 75 mg quartz as a function of time on stream. The CO/O_2 reactant feed ratio was 2:1 at atmospheric pressure and the reaction temperature was 393 K [46].

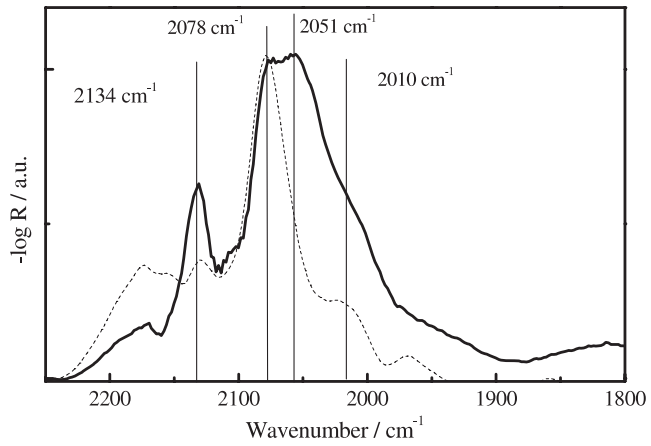

Figure 16. DRIFT spectra at atmospheric pressure [30] during the oxidation of CO CO/O_2 feed ratio of 4:1 (solid), and 1:2 (dotted) over Ru/SiO_2. The DRIFT spectra were recorded at 423 K.

Pt(110) [44]. For the following discussion these oscillations are not important, but rather we focus on the severe decay of CO conversion with time on stream. Already the long time scale of deactivation indicates that structural deactivation may be operative. Alternative sources of deactivation can be ruled out, as reversible poisoning for instance by water or carbonate species at low temperatures takes place on a much shorter time scale, typically 30 min [8, 9, 45, 48]. Sintering of the catalyst particles associated with a reduction of the active surface area can equally be ruled out by TEM and H_2 chemisorption measurements, which show that the Ru dispersion is only slightly changed under various reaction conditions.

In order to determine the chemical state of the exposed surfaces of the supported Ru particles under CO oxidation reaction conditions we applied *in situ* DRIFT spectroscopy. In figure 16 we present DRIFT spectra in the carbonyl region for a fixed CO/O_2 feed ratio of 4:1, i.e. under net reducing reaction conditions at 423 K. Gaseous CO_2 was identified by the bands at 2340 and 2360 cm^{-1} [30]. The higher the reaction temperature was, the higher the CO_2 signal in the DRIFT spectra consistent with an increased CO conversion rate. In the carbonyl region three bands are observed in figure 16 at 2134, 2078, 2051 cm^{-1}, and a shoulder at 2010 cm^{-1}. In comparison with HREELS experiments of $RuO_2(110)$ [39] and with RAIRS measurements of $RuO_2(110)$, the 2134 cm^{-1} feature is assigned to on-top CO on cus Ru, while the shoulder at 2010 cm^{-1} is ascribed to (asymmetric) bridging CO. The 2070 cm^{-1} signature belongs to a concerted vibration of on-top CO and bridging CO [38]. These features demonstrate that the Ru particles are covered by RuO_2, where the bridging O atoms are replaced by adsorbed CO molecules. On the other hand, the absorption feature at 2051 cm^{-1} is a clear signature of on-top CO adsorbed of metallic Ru. In summary, the catalyst surface exposes both metallic Ru and mildly reduced RuO_2 domains under net reducing reaction conditions.

When switching the flow from a feed with a CO/O_2 ratio of 4:1 to a feed with a CO/O_2 ratio of 1:2, the most obvious change in the spectra is the disappearance of the 2051 cm^{-1} feature which is assigned to CO on metallic Ru disappears. The RuO_2-related CO features shift slightly in wavenumber, but can still uniquely be assigned to on-top CO (2134 cm^{-1}), bridging CO (2010 cm^{-1}), and dense domains of on-top CO/bridging CO (2073 cm^{-1}) on RuO_2. The intensity of the on-top CO species is much smaller under oxidizing reaction than under reducing reaction conditions. This is consistent with the fact that CO and O_2 compete for the same cus Ru sites. In conclusion, these DRIFTS data imply that the catalyst surface consists exclusively of RuO_2 under net oxidizing reaction conditions.

In order to determine the bulk composition of the working Ru/SiO_2 catalysts running under oxidizing or reducing reaction conditions, we performed additional TPR measurements in hydrogen in the same reactor used for catalytic testing. For reducing reaction conditions TPR measurements reveal that the observed hydrogen consumption is solely related to methane production (the carbon is originating from the CO adsorption) and not to water production. Therefore, under reducing reaction conditions the Ru/SiO_2 catalyst is considered to be essentially metallic within the detection limit of the TPR flow set-up. Combined with DRIFTS, which is probing the surface composition, we arrive at a core–shell model for the catalyst under reducing reaction conditions, namely that the core consists of metallic Ru which is only partly covered by an ultrathin RuO_2 film. For the Ru/SiO_2 catalyst running under oxidizing reaction conditions, TPR experiments reveals pronounced water production around 400 K. Since the total amount of ruthenium is known, we can determine a Ru:O stoichiometry of 1:2, i.e., fully oxidized RuO_2.

From these experiments with applied Ru-based catalysts we conclude that the deactivation process of Ru/SiO_2 during the CO oxidation reaction under reducing conditions is due to the presence of metallic Ru domains on the exposed surfaces of the Ru particles. Metallic ruthenium is known to be a poor catalyst for the CO oxidation. Under oxidizing reaction conditions, however, the Ru/SiO_2 catalyst becomes fully oxidized. The deactivation of Ru/SiO_2 under oxidizing reaction conditions is quite puzzling, as recent investigations clearly indicate that RuO_2 is very active in the oxidation of

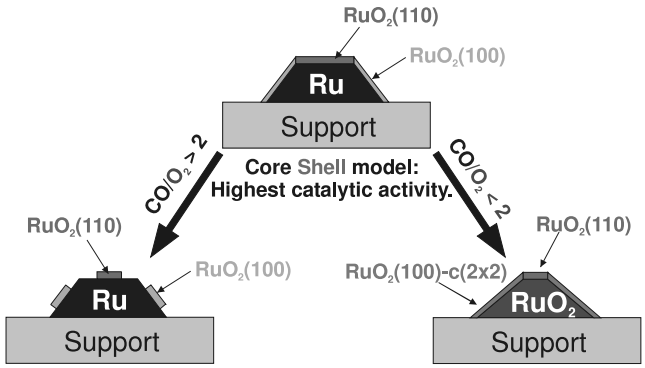

Figure 17. Structural deactivation of supported RuO_2 catalysts during CO oxidation under reducing and oxidizing reaction conditions.

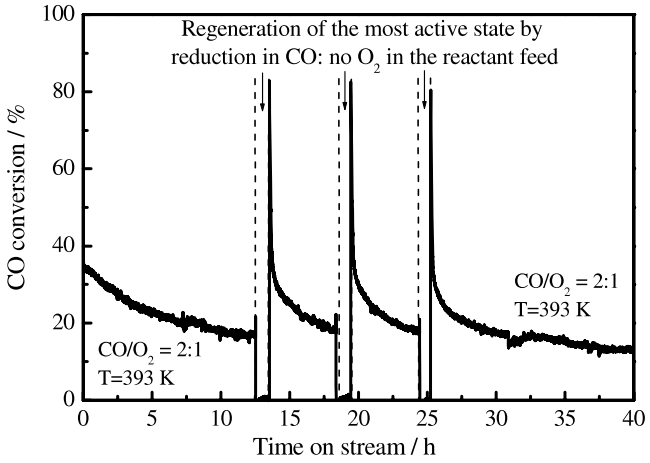

Figure 18. Steady-state CO oxidation at 393 K using a stoichiometric CO/O_2 gas feed ratio of 2:1. For restoring the high catalytic activity the catalyst is periodically reduced for 1 h in CO with constant concentration of CO by switching off O_2 and increasing the flow of Ar [46]. In this experiment the restoration of the catalyst was performed three times.

CO. However, since the pressure and materials gaps for the oxidation of CO over Ru are considered to be bridged we can utilize the surface science approach to clarify the microscopic processes, determining the structural deactivation of Ru-based catalysts under oxidizing reaction conditions and transferring this atomic scale knowledge to optimize the performance of applied Ru catalysts.

In the following we summarize briefly those experiments which indicate deactivation of RuO_2 model catalysts (surface science approach), and how we transferred this knowledge to practical Ru catalysts. First of all, on $RuO_2(100)$ we identified a unique c(2 × 2) phase which is inactive in CO oxidation. But also a $RuO_2(110)$ film can deactivate, when the oxidation conditions are quite harsh, that is, when the oxidation temperature is beyond 700 K. Under these circumstances the $RuO_2(110)$ roughens considerably (cf STM image in figure 1), and TDS experiments indicate that CO and O_2 adsorption is inhibited. This experimental evidence indicates that even the (110) orientation of RuO_2 deactivates under oxidizing reaction conditions. A closer look of such a roughened $RuO_2(110)$ surface (STM image in figure 1) shows that the observed facets expose preferentially inactive c(2 × 2) areas. This is further evidence that the c(2 × 2) phase is responsible for the observed deactivation of RuO_2 catalysts under oxidizing reaction conditions, both for model as well as applied catalysts.

The deactivation mechanism for supported Ru catalysts during CO oxidation is summarized in figure 17. Under reducing reaction conditions the active RuO_2 particle becomes chemically reduced, exposing inactive metallic Ru patches. Under oxidizing reaction conditions the Ru particle is fully oxidized and exposes inactive c(2 × 2) areas. More specific, the RuO_2 particles expose preferentially (110) and (100) facets. Upon CO oxidation under net oxidizing conditions, the active $RuO_2(100)$ facets of the RuO_2 particle transform into the inactive $RuO_2(100)$-c(2 × 2) phase. But also the $RuO_2(110)$ facets will deactivate partly under oxidizing conditions. The $RuO_2(110)$ facets roughen considerably, thereby forming additional $RuO_2(100)$ facets (compare figure 1), which reconstruct into the inactive c(2 × 2) phase. Both deactivation processes are the more efficient the higher the temperature is, consistent with the deactivation behavior of RuO_2 powder and supported Ru catalysts. Finally, the RuO_2 particle exposes predominantly catalytically inactive $RuO_2(100)$-c(2 × 2) facets and only small areas of active $RuO_2(110)$ facets. The deactivation scheme summarized in figure 17 is equally valid for RuO_2 powder catalysts [22].

3.2. How to avoid structural deactivation of RuO_2? Preparation of structurally stable RuO_2 catalysts

The supported Ru catalyst is able to adjust the surface composition according to the actual reaction conditions during CO oxidation. Under reducing reaction conditions the RuO_2 particle reduces partly, while under oxidizing reaction conditions the RuO_2 particles exposes inactive c(2 × 2) patches. From this observation, the easiest way to mitigate structural deactivation would be to switch periodically between oxidizing and reducing reaction conditions. Indeed, as shown in figure 18, such a transient way of operating the fixed-bed reactor is able to keep the RuO_2 catalyst in a more active state.

An alternative approach to keep the RuO_2 catalyst in the chemically active state is demonstrated with the microscale RuO_2 powder catalyst. Again, we identify the means by transcribing the knowledge from the surface science approach to the practical RuO_2 catalyst. We know that ultrathin RuO_2 films both on Ru(0001) and on Ru(10$\bar{1}$0) are extremely active in the oxidation of CO and that these RuO_2 films grow self-limiting with a thickness of 1.6 nm. We know also that for reaction temperatures below 650 K these active RuO_2 films are stable under oxidizing reaction conditions. This suggests the following recipe to prepare an efficient and stable RuO_2 powder catalyst. First, we fully reduce the RuO_2 particles to metallic Ru by exposing the catalyst to flowing H_2 at 750 K. Then we re-oxidize the Ru particles under gentle reaction conditions, say temperatures below 500 K. This procedure indeed results in a very active and also stable RuO_2 powder

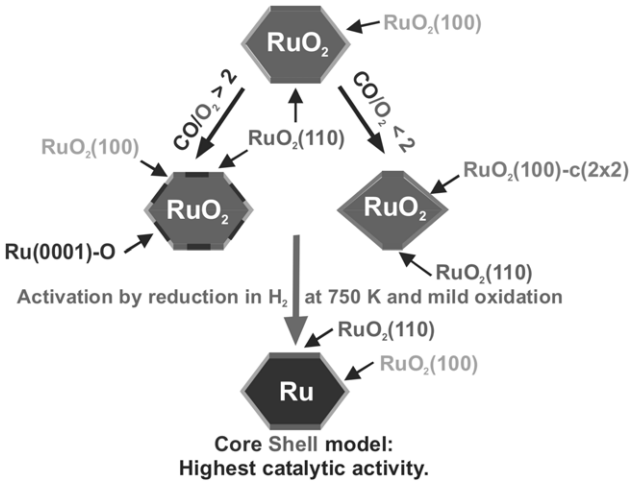

Figure 19. Core–shell model for RuO_2 powder catalysts: The degree of surface oxidation is determined by the CO/O_2 reactant feed ratio and the temperature. The inactive $RuO_2(100)$-c(2 × 2) surface facets are formed under oxidizing conditions ($CO/O_2 < 2$), whereas low activity metallic Ru surfaces (Ru(0001)–O) are exposed under net reducing conditions ($CO/O_2 > 2$). The most active state is an ultrathin RuO_2 layer supported on a metallic Ru core which is accomplished by complete reduction of the RuO_2 particle followed by a mild re-oxidation below 500 K [9, 22].

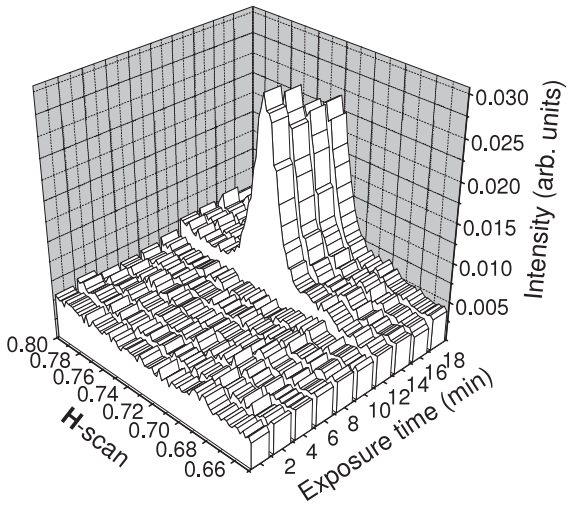

Figure 20. *In situ* SXRD experiment: oxidation of the Ru(0001) sample by exposing it to a gas mixture of O_2 and CO: $p(O_2) = 18$ mbar, $p(CO) = 10$ mbar at a sample temperature of 630 K; evolution of the **H** scan as a function of exposure [11].

catalyst (cf figure 19). The oxidation state of this catalyst is determined by TPR. Only little oxygen is present in/on the Ru particle consistent with a Ru particle that is covered only by an ultrathin RuO_2 layer (core–shell model).

We can safely assume that the metallic Ru particles in the fully reduced RuO_2 powder catalyst expose preferentially (0001) and $(10\bar{1}0)$ facets, since those are the surfaces with lowest surface energies (compare the Wulff construction in the supporting material of [22]). Under mild reaction conditions the Ru particle will oxidize by growing a 1–2 nm thick $RuO_2(110)$ layer on the Ru(0001) facets and a $RuO_2(100)$ layer on the Ru$(10\bar{1}0)$ facets. This RuO_2/Ru shell–core particle reveals the highest activity in the CO oxidation (cf figure 19).

The stability of this RuO_2/Ru shell–core particle is controlled by kinetics. For Ru particles with a mean diameter of 1 μm (reduced RuO_2 powder) or for the macroscopic Ru(0001) and Ru$(10\bar{1}0)$ single crystals, the oxidation of Ru stops at a thickness of 1.6 nm when the temperature does not exceed 650 K. Therefore, the active state of the reduced RuO_2 powder catalyst is maintained under oxidizing reaction conditions. In contrast, for supported Ru catalysts the nanoscale Ru particles (typical size of 2–3 nm) with active $RuO_2(110)$ and $RuO_2(100)$ layers surrounding the metallic Ru core are unstable under both reducing and oxidizing reaction conditions. Either the nanoparticle is reduced, exposing inactive Ru domains, or it is oxidized completely, exposing predominantly inactive c(2 × 2) domains. The supported Ru catalyst is expected to work more stable for larger Ru particles. The high catalytic activity is, however, balanced by the inferior surface/bulk ratio of larger particles, so that an optimum particle size is expected to be somewhat higher than 10 nm.

The turnover frequencies (TOF) of pre-reduced RuO_2 powder catalyst and that of the pre-oxidized RuO_2 powder are compared to those of the active state and the inactive state of RuO_2 as summarized in figure 14. Clearly, the pre-reduced RuO_2 powder is in the catalytically active state, while the pre-oxidized RuO_2 powder catalyst behaves as the deactivated RuO_2 catalyst.

3.3. Shell–core model for the active $RuO_2(110)$/Ru(0001) catalyst

For the supported Ru catalyst and the pre-reduced RuO_2 powder catalyst the most active state Ru for the CO oxidation consists of particles of a metallic Ru core that is coated by an ultrathin RuO_2 film. Is this also true for the model catalyst Ru(0001)? To answer this question, *in situ* SXRD experiments were performed while dosing CO and O_2 with 1:2 CO:O_2 gas mixture [11]. The reaction temperature was chosen to be 630 K, i.e. beyond the threshold temperature of 500 K to ensure oxide formation. With a mixture of CO and O_2 of up to 10 mbar in total pressure no oxidation of the Ru(0001) was observed with *in situ* SXRD. However, when we increased the total CO + O_2 pressure to 28 mbar, after an induction period of 700 s the oxidation of Ru(0001) set in spontaneously and was completed within one single **H** scan (i.e. within 100 s) (cf figure 20). The H scan probes the lateral surface periodicity, while the L scan probes the vertical structure of the $RuO_2(110)$ film. From the FWHM of the Bragg peaks in the **L** scan (not shown) the averaged thickness of the $RuO_2(110)$ domains is derived to be 1.6 nm [11].

The long induction period together with the high total pressure of 28 mbar required to oxidize the Ru(0001) sample suggests that the oxidation of the first RuO_2 domain imposes the rate determining step for the oxidation of Ru(0001). It seems that a critical size of a RuO_2 nucleus is needed to initiate the oxidation of the first RuO_2 domain. The formation of such a

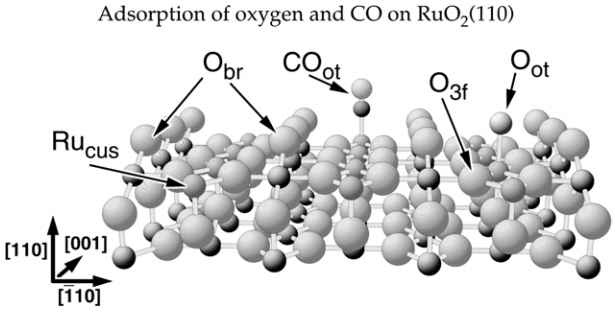

Figure 21. The adsorption of CO and oxygen on the stoichiometric $RuO_2(110)$ surface. Both adsorbates occupy the on-top positions above the cus Ru atoms.

RuO_2 nucleus is subject to reduction by CO, so that the critical size of the nucleus is only stable when the pressure of O_2 is high enough. This CO + O_2 experiment confirms nicely that also for the Ru(0001) surface, serving as the model catalyst, we identify a core–shell model, in which the Ru(0001) surface is covered by a self-limiting grown $RuO_2(110)$ film, whose thickness is 1.6 nm.

4. Microscopic reaction steps in the catalytic CO oxidation over RuO_2

4.1. General adsorption properties of RuO_2

Oxygen exposure to the stoichiometric $RuO_2(110)$ surface leads to the population of the atomic oxygen adsorbed on top of the cus Ru atoms [26] (see figure 21). Exposure of 5 L of O_2 at room temperature saturates 80% of the cus Ru atoms by on-top O atoms (O_{ot}). Exposure of CO at low temperatures (e.g. 200 K) results also in the occupation of the cus Ru atoms by upright sitting CO molecules (see figure 21). Therefore, oxygen and CO compete on the stoichiometric $RuO_2(110)$ surface for the same adsorption sites, at least at low surface temperatures (below 250 K).

Most of the molecules studied so far on the $RuO_2(110)$ surface (CO [47], H_2O [49], O_2 [26], N_2 [47], methanol [50], CO_2 [51], NO [52], ethylene [53], and NH_3 [54]) adsorb from the gas phase directly above the cus Ru atoms. Therefore, the cus Ru atoms are considered to be the dominating active sites of $RuO_2(110)$ governing the interaction with the gas phase [55]. So far only hydrogen molecules have been shown to interact also with the bridging O atoms above 150 K mediated by the adsorption on the cus Ru atoms, forming bridging hydroxyl groups [56–59].

4.2. The CO oxidation reaction: experimental evidence

The high catalytic activity of stoichiometric $RuO_2(110)$ towards CO oxidation was demonstrated on the atomic scale to be controlled by the presence of cus Ru atoms [55]. We stress this important point since not defects, but rather the regular, undercoordinated surface atoms govern the activity of RuO_2. On the stoichiometric $RuO_2(110)$ surface, CO molecules adsorb strongly (adsorption energy exceeds 120 kJ mol^{-1} [37]) on top of the cus Ru atoms (cf figures 21 and 23), from where the actual oxidation reaction takes place via recombination with undercoordinated surface oxygen atoms (either bridging O or on-top O atoms). Recent high resolution energy electron loss spectroscopy (HREELS) measurements [39] and STM experiments [60] have essentially confirmed this view, and DFT calculations characterized the transition states of these reaction pathways [28, 61–63] (cf also section 4.3).

For the following discussion the sample temperature is chosen to be between 350 and 400 K. This surface temperature is high enough to ensure facile CO oxidation, but also low enough to prevent the surface from restructuring. Under oxidizing reaction conditions, i.e., with CO and excess O_2 in the gas feed, the $RuO_2(110)$ surface offers the adsorbed CO molecule two potentially catalytically active oxygen species to form CO_2. In addition to the bridging O atoms, the $RuO_2(110)$ surface stabilizes an on-top oxygen species (see figure 22) which is by 150 kJ mol^{-1} more weakly bound to RuO_2 than the bridging O atoms [26]. Chemical intuition would therefore anticipate that the on-top O species dominates the activity of $RuO_2(110)$, a conclusion that was apparently supported by HREELS measurements [40]. However, careful isotope labeling experiments with ^{18}O have shown that the bridging O species is practically as active in oxidizing CO as the on-top O species [64]. Density functional theory (DFT) calculations attribute this counterintuitive finding to an activation energy that is almost degenerate for the CO recombination with on-top O and bridging O (cf section 4.3). Under strongly oxidizing reaction conditions, the removed bridging O atoms are replenished by on-top O atoms. Therefore, on average the bridging O rows are intact and CO sits preferentially on top of cus Ru sites.

Under strongly reducing reaction conditions, i.e. with excess CO in the gas feed, both reactants adsorb initially over the cus Ru atoms and the adsorbed CO molecules easily recombine with bridging O atoms (O_{br}) or with on-top O (O_{ot}) to form CO_2. In principle, the reacted-off bridging O atoms can by replenished by on-top O originating from the dissociative adsorption of molecular oxygen from the gas phase. However, since CO is in excess most of the reacted-off bridging O atoms will subsequently be replaced by strongly adsorbed bridging CO molecules (1.75 eV) [37]. After an induction period most of the bridging O atoms are replaced by bridging CO molecules, and the actual reaction takes mainly place between on-top CO and on-top O. We should mention that the strongly adsorbed bridging CO stabilizes the RuO_2 against further reduction as long as the reaction temperature is below 400 K.

Under stoichiometric reaction conditions, that is, when the ratio of CO and O_2 in the gas feed is 2:1, part of the bridging O atoms are replaced by bridging CO. CO can in principle react with both oxygen species, the on-top O and the remaining bridging O species. Under steady-state reaction conditions the mean concentrations of bridging O and bridging CO are constant.

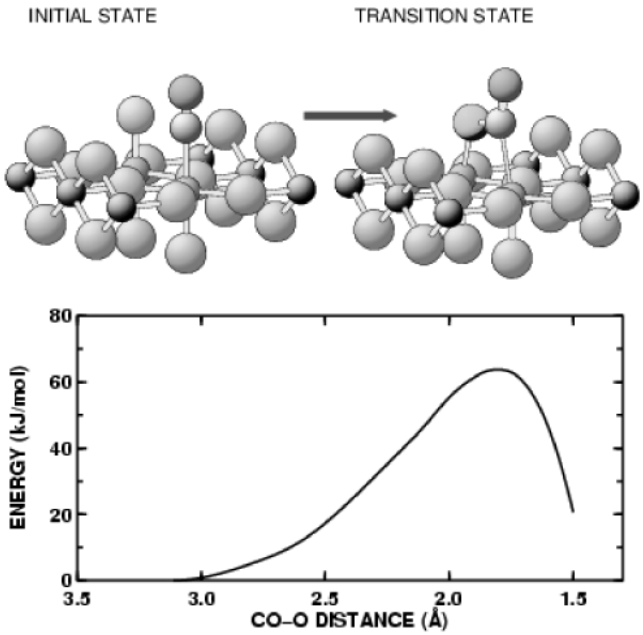

Figure 22. Top: stick and ball model of the initial and transition state of on-top CO and on-top O, reacting on the $RuO_2(110)$ surface. Large balls represent oxygen and small balls ruthenium atoms. Bottom: energy along the recombination reaction of on-top CO with on-top O.

4.3. The CO oxidation reaction: DFT calculations of elementary steps

The DFT calculations were carried out by using the VASP code applying the improved pseudopotentials for Ru and O.[5] These new pseudopotentials have demonstrated to be reliable and consistent with corresponding FLAPW calculations [66]. The $RuO_2(110)$ surface is modeled by five trilayers of RuO_2 with a (1×2) surface unit cell (super cell approach). 20 Å of vacuum is used to ensure a vanishing interaction between the two surfaces of the slab via the vacuum. We define the reaction coordinate as the O–CO separation between the reacting species on the surface. The transition state (TS) of each reaction pathway and the corresponding activation barrier $\Delta E^{\#}$ is searched using a constrained minimization technique. The TS are identified as the configuration at a specific CO–O distance, where the forces on the atoms vanish and the energy reaches a maximum along the reaction coordinate. Within statistical thermodynamics the activation entropy $\Delta S^{\#}$ is given by the quotient of the partition functions of the TS and the initial state (IS), requiring the *ab initio* calculations of the vibrational frequencies of the reactants in both the IS and the TS [67].

The $RuO_2(110)$ surface provides the catalytic CO oxidation reaction with two potentially active oxygen species. Besides the bridging O atoms, the $RuO_2(110)$ surface stabilizes an on-top oxygen species (see figure 21) which is by 150 kJ mol^{-1} more weakly bound than the bridging O atoms [26, 68].

In modeling the CO oxidation reaction over $RuO_2(110)$, we concentrated first on the initial state (IS), in which the CO molecule resides in on-top position above the cus Ru atoms and the active oxygen species on the surface is placed on the on-top position next to the CO molecule (cf figure 22). Our DFT calculations determine the activation energy for the recombination of on-top CO with on-top O to be 71 kJ mol^{-1}. The atomic geometry of the transition state is illustrated in figure 22: both CO and the adjacent O_{ot} atom are displaced from their initial adsorption sites along the [001] direction, respectively. During the recombination process substantial distortions of the O_{3f} positions occur in the topmost Ru–O trilayer. These relaxations of the $RuO_2(110)$ surface are mandatory for a reliable determination of the activation energies.

In the second elementary reaction step the initial state (cf figure 23) is defined by the CO molecule again residing in on-top position above the cus Ru atoms and the active oxygen species on the surface is the bridging O atom. DFT calculations determine the activation barrier to be 74 kJ mol^{-1}, which is only 3 kJ mol^{-1} higher in energy than for the recombination of on-top CO and on-top O. The calculated activation entropy for the case of on-top CO/on-top O reaction pathway is -68 and -50 J K^{-1} mol^{-1} for the on-top CO/bridge O reaction route. Therefore, the free activation energies for the reaction of adsorbed CO molecules on $RuO_2(110)$ with bridging oxygen and with on-top oxygen at 300 K is virtually degenerate: the smaller decrease of activation entropy outweighs the slightly higher activation barrier of CO with bridging O atoms in comparison with on-top O.

We compare in table 4 our DFT-derived values of the activation barriers with corresponding values of previous first principles calculations [66, 68, 69]. Clearly, the activation barriers scatter markedly among these studies. Most remarkably, in contrast to our DFT calculations the activation barriers of the association of on-top CO with on-top O and bridging O in [68, 69] differ by 20–40 kJ mol^{-1}. This finding implies that both reaction pathways should readily be resolved in temperature-programmed reaction experiments, incompatible with recent experimental findings [62, 64]. The activation energy for the recombination of on-top CO and on-top O of our study is practically identical to that of Kiejna *et al* [66]. The major discrepancy occur for the activation energy of on-top CO with bridging O. Using the structural parameters of the TS of Kiejna *et al* we recalculated the activations barriers

Table 4. Activation energy (kJ mol^{-1}) for the recombination of the on-top CO with bridging O and with on-top O over $RuO_2(110)$ as determined by various DFT calculations.

Reaction barrier	This study	Ref. [68]	Ref. [69]	Kiejna *et al* [66]	Recalculating Kiejna *et al*
On-top CO/ on-top O	71	86	64	74	73
On-top CO/ bridging O	74	121	111	94	92

[5] The calculations were performed with the program VASP (Kresse and Furthmüller [65]) and employing the projected augmented wave, PAW (Blöchl [65]), approach in the variant of Kresse and Joubert (Kresse and Joubert [65]), to describe the action of the core electrons on the valence electrons and to remove the divergence in the external potential. A cut-off energy of 37 Ryd was applied.

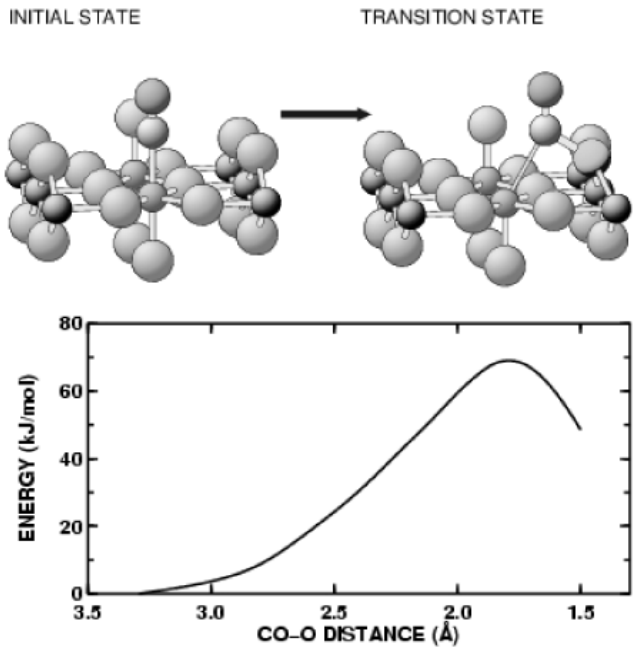

Figure 23. Top: stick and ball model of the initial and transition state of on-top CO and bridging O reacting on $RuO_2(110)$ surface. Bottom: energy along the reaction coordinate, i.e. recombination reaction of on-top CO with bridging O.

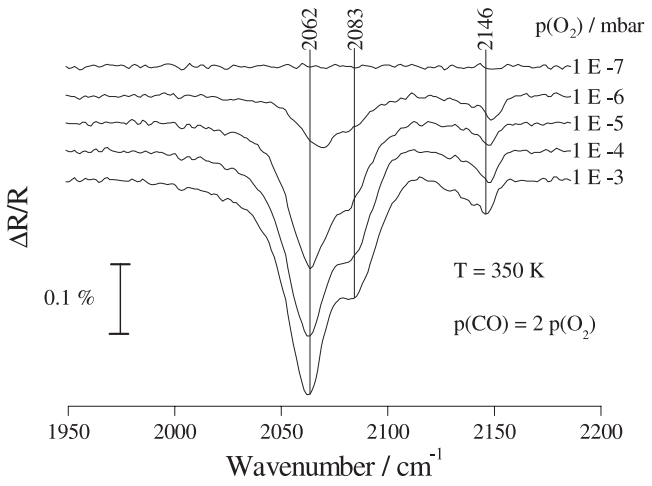

Figure 24. *In situ* RAIRS spectra during the CO oxidation reaction over the model catalyst $RuO_2(110)$ at 350 K with a reactant feed $p(CO) = 2 \times p(O_2)$ with varying pressure ranging from 10^{-7} to 10^{-3} mbar [38].

for both reaction pathways and indeed with the TS geometries of Kiejna *et al* we arrive at a virtually identical activation energy (cf table 4). These control calculations clearly indicate that the discrepancy of the activation energies is related to the differing geometry of the TS for the reaction between on-top CO and bridging O. Since our activation energy is lower, the optimized TS geometry is more reliable than that presented in the literature [66, 68, 72, 73]. We performed also some additional DFT calculations to identify the reason, why the reaction of on-top CO with bridging O and on-top O is quasidegenerate. It turned out that the promotion of the CO molecule is the decisive step in the recombinative reaction of CO and O on the $RuO_2(110)$ surface. A detailed discussion will be presented in a forthcoming paper [70].

Other possible reaction pathways between CO and O on the $RuO_2(110)$ have already thoroughly been discussed [28, 62, 63] and later confirmed [68, 71]. Adsorbed CO can migrate into bridging O vacancies, thereby producing strongly bonding bridging CO molecules. These bridging CO can react either with bridging O or with on-top O. The corresponding activation barriers are determined to be 140 kJ mol^{-1} and 60 kJ mol^{-1}, respectively [63]. Therefore the recombination of bridging O and bridging CO is of no relevance for the actual reaction mechanism. Quite in contrast, the activation barrier between bridging CO and on-top O is the lowest among the possible elementary reaction pathways, thus may be relevant for the reaction mechanism. A detailed discussion, which elementary reaction pathways are important in the CO oxidation reaction mechanism over $RuO_2(110)$, is discussed in section 4.4.

4.4. First principles kinetic Monte Carlo simulations for the CO oxidation on $RuO_2(110)$

The microkinetic modeling of the steady-state CO oxidation reaction over $RuO_2(110)$ has been performed by kinetic Monte Carlo (MC) simulations [72]. The input parameters to such kinetic MC simulations are the rate constants of all elementary processes that can take place on the surface, including adsorption, desorption, diffusion and chemical reactions. The rate constants were calculated using transition state theory with activation energies provided by *ab initio* theory. Since the activation barriers for the most important reaction steps, namely the recombination of CO with bridging O and with on-top O are still a matter of discussion (cf section 4.3), the conclusions drawn from kinetic MC simulations [72] have to be considered with caution. We should mention that most of these *ab initio* calculated quantities entering the kinetic MC simulations had already been known in literature [28]. However, combining these values into a kinetic MC scheme to simulate the CO oxidation reaction mechanism over $RuO_2(110)$ provides an important step towards an atomic scale understanding of catalysis, since the complex interplay of various restrictions, coming from diffusion barriers of the reactants and the blocking between the on-top CO and on-top O are properly considered.

The diffusion barriers for on-top O and on-top CO along the cus Ru rows are quite high amounting to about 100 kJ mol^{-1}, while diffusion perpendicular to the cus Ru rows into O bridge vacancies is activated by only 70 kJ mol^{-1} [28]. Therefore, both CO molecules and on-top O atoms can easily hop from the cus Ru atoms into the O_{br} vacancies, thereby increasing their binding energies to the surface by 50 kJ mol^{-1} and 140 kJ mol^{-1}, respectively [62, 63]. The highly activated diffusion processes are important for the kinetics at moderate reaction temperatures. According to kinetic MC simulations [71], the most efficient reaction step between bridging CO and on-top O does not occur, since the population of bridging CO is under typical gas

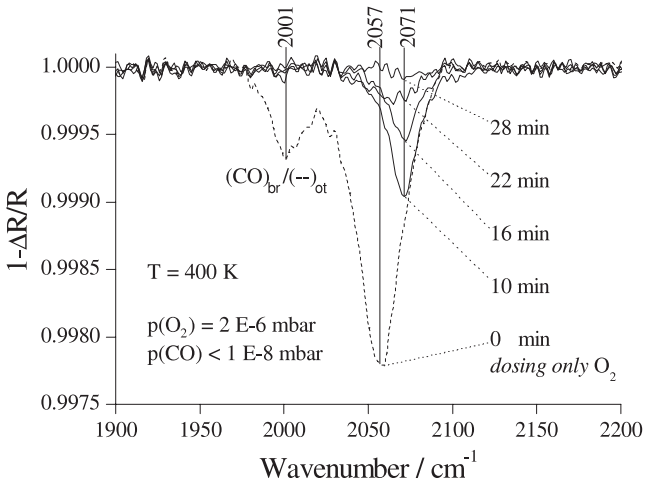

Figure 25. RAIRS experiments showing the partial self-poisoning of the $RuO_2(110)$ model catalyst by the reactant CO. First, CO and O_2 were exposed to the surface at $p(CO) = 3 \times p(O_2) = 6 \times 10^{-6}$ mbar at $T = 400$ K. Then, the CO flux was switched off and the residual CO species were monitored by RAIRS [38].

feed stoichiometries negligibly small. The most important elementary reaction step is considered to be the recombination between on-top CO and on-top O due to the low energy barrier. Note that this reasoning is questionable according to the discussion in section 4.3 and new RAIRS experiments (see below). Due to high diffusion barriers of the surface species and due to a complex interplay of adsorption and desorption and that of vacancy creation during the catalyzed reaction, inhomogeneities with strongly varying concentrations of the reactants are formed on the surface, which do not allow for the application of simple mean-field approximations [71].

With *in situ* infrared spectroscopy we were able to follow the status of the catalytically active $RuO_2(110)$ surface during the CO oxidation reaction [38]. Such RAIRS experiments are presented in figure 24. The CO molecule serves as both the reactant in the CO oxidation reaction and as the probe molecule to study the chemical nature of the surface. The gas feed ratio of $CO:O_2$ was 2:1, and the reaction temperature was 350 K. The RAIRS spectrum in figure 24 is dominated by an absorption band at 2062 cm^{-1}. This feature has been assigned to CO in domains with dense bridging CO and open on-top CO chains. The shoulder at 2083 cm^{-1} is assigned to a dense CO domain of bridging and on-top CO. The CO vibration at 2145 cm^{-1} is ascribed to on-top CO in an oxygen matrix of bridging and on-top O. As can be seen in figure 24 the RAIRS spectra do not change very much above 10^{-6} mbar, when the total pressure is increased by 3 orders of magnitude. However, at 10^{-7} mbar, nearly no signal from adsorbed CO is seen in the spectrum. Obviously, the CO oxidation process is so fast that the mean CO concentration on the surface is quite low. According to this experiment, results at 10^{-7} mbar are not transferable to higher pressures.

In the *in situ* RAIRS experiment shown in figure 25 the gas feed was chosen to be $p_{CO} = 3 \times p_{O_2} = 6 \times 10^{-6}$ mbar, i.e. strongly reducing reaction conditions, and the reaction temperature was kept at 400 K. Again, this spectrum is dominated by a single vibration at about 2060 cm^{-1}, which is assigned to CO in a domain where the bridging CO molecules form dense rows and the on-top CO is sparsely populated. At the high energy flank of this peak there is a shoulder at 2071 cm^{-1} which is assigned to CO in dense domains, with both on-top and bridging rows are densely packed. The vibrational band at 2001 cm^{-1} is related to bridging CO without any adsorbate on neighboring on-top sites. Subsequently, the gas feed was switched to strongly oxidizing conditions by closing the CO leak valve. Still a pronounced CO related feature persists in the RAIRS spectrum, indicating that this CO species can only hardly be oxidized even when excess oxygen is applied. This means that we are monitoring a CO species which is inactive in the CO oxidation reaction; in other words this CO species is poisoning the catalyst. Since these inactive species is CO located in dense CO domains, CO oxidation can only proceed at the perimeter of such domains by recombination of neighboring on-top O with CO. This leaves free single cus Ru sites at the perimeter of the CO domains, in which oxygen adsorption directly from the gas phase can hardly take place, as O_2 dissociation requires at least two neighboring free cus Ru sites.

Furthermore, the diffusion of CO and/or on-top O is hindered by the high diffusion barriers of about 100 kJ mol^{-1}. Altogether these restrictions let the densely CO domains exist on the $RuO_2(110)$ surface for a time period of 20 min. We should emphasize that this inactive CO spectator species with a characteristic vibration at 2070 cm^{-1} is observed on both the model catalyst (RAIRS) and on the supported Ru catalysts (DRIFTS) (cf figure 12). This experimental result is not appropriately reconciled by kinetic MC simulations [71], since the activation energy for the recombination of bridging O and on-top CO is assumed too high. Therefore, the replacement of bridging O by CO is hindered and under typical reaction conditions not observed in these kinetic MC simulations.

4.5. Microscopic reaction steps in the catalytic CO oxidation over polycrystalline RuO_2 powder

We are now able to investigate the steady-state kinetics of CO oxidation, because we can generate the active state of the catalyst without facing the problem of deactivation during the reaction. Ongoing deactivation during the catalytic reaction would render these experiments impossible. Achieving a stable and catalytically active state by the reductive pretreatment allows a microkinetic analysis of the conversion data as a function of temperature and gas-phase composition both for the microscale RuO_2 powder as well as for the nanoscale RuO_2 powder, the latter requiring an extended pretreatment to be reported elsewhere [35].

4.5.1. Probing the active RuO_2 surface by TPD of adsorbed CO and O: comparison between RuO_2 powder and the RuO_2 single-crystal surface. To discriminate different reaction pathways (described in section 4.3) temperature-programmed desorption (TPD) experiments were performed with polycrystalline RuO_2 powder and RuO_2 single crystals. Depending on either reductive or oxidative pretreatment of the polycrystalline RuO_2 sample it was possible to achieve

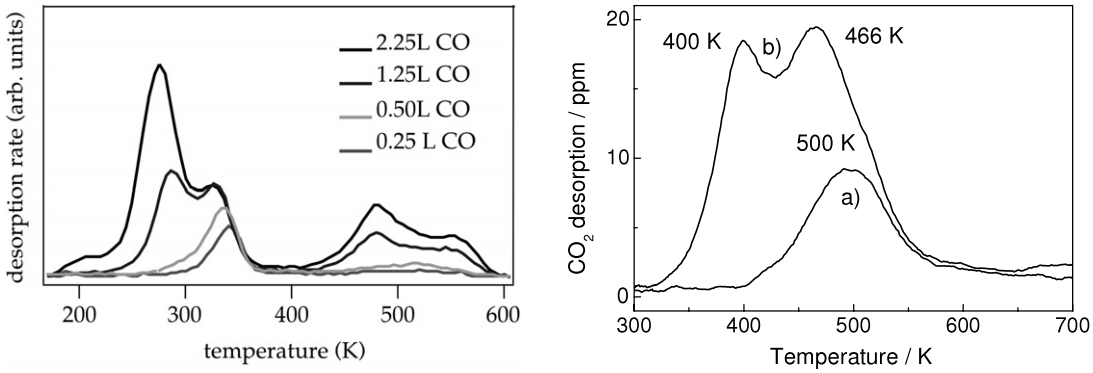

Figure 26. CO_2 production during TPD of adsorbed CO and O from a single-crystalline RuO_2(110) film (left), in comparison with polycrystalline RuO_2 (right). The CO_2 TPD spectra (right) were obtained after oxidation of CO at 450 K over pre-reduced polycrystalline RuO_2 under an excess of oxygen ($CO/O_2 = 0.5$). The TPD measurements were performed with He as carrier gas after the sample was cooled down in (a) 20% O_2/Ar mixture and (b) the CO/O_2 reaction mixture.

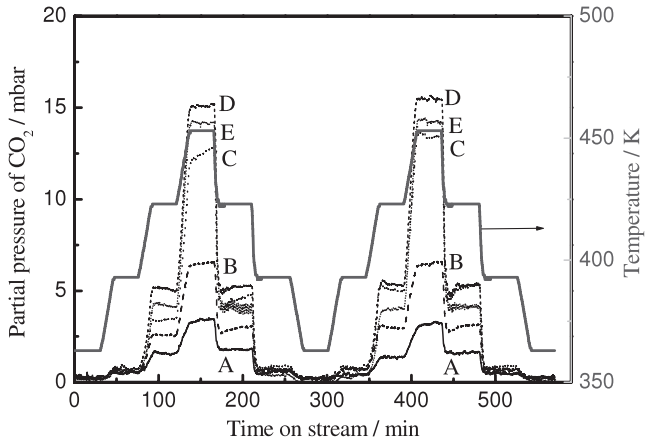

Figure 27. Partial pressure of CO_2 measured during the oxidation of CO over 12.5 mg RuO_2/Ru powder obtained by H_2 reduction of microscale RuO_2 at 723 K, diluted with 100 mg of silica, as function of time and temperature. The temperature program is displayed by the light gray trace. Variation of the CO/O_2 reactant ratio with a constant partial pressure of O_2 (9.1 mbar): (A) 0.5, (B) 1, (C) 2, (D) 4, (E) 6.

different states of the catalyst surface yielding different reaction performances due to varying CO/O coverage ratios. First, RuO_2 powder was reduced in H_2 at 773 K, followed by the oxidation of CO under an excess of O_2 (CO/O_2 reactant feed ratio = 0.5) at 450 K with a CO conversion in the range of 70%. After these two steps the subsequent cooling procedure was carried out either in the reaction mixture or in an oxygen/argon gas mixture, leading to different CO_2 desorption profiles which are shown in figure 26.

The TPD measurements using He as carrier gas reveal two CO_2 desorption signals at 400 and 466 K after cooling the sample down to room temperature in the CO/O_2 reactant feed mixture, but only one peak at 500 K, when the sample was cooled down in the O_2/Ar gas mixture. One possible reason for this different behavior is that cooling down in O_2 removes all active CO molecules, and only strongly bound CO remains on the RuO_2 surface. Cooling down in the CO/O_2 reaction mixture opens also the low temperature reaction pathway which means that CO is adsorbed on two different sites. Regarding the results of the single-crystal studies (figure 26, left) and DFT calculations (section 4.3), the reaction pathways are identified with the reaction between on-top CO and O_{br}/O_{ot} at low temperatures and the recombination of bridging CO and bridging O at 500 K. This excellent agreement of the results obtained for model systems and for powder catalysts once more demonstrates that the materials and the pressure gaps are closed.

4.5.2. Steady-state oxidation of CO over RuO_2 powder: reaction orders of CO and O_2. With polycrystalline microscale RuO_2 we identified a material that suppresses a strong re-oxidation under reaction conditions after it had been initially reduced to metallic Ru powder. Thus, for the first time we had the opportunity to investigate detailed kinetics for the oxidation of CO over RuO_2/Ru catalysts at atmospheric pressure without the negative influence of ongoing deactivation phenomena.

The results of the catalytic activity measurements performed with polycrystalline RuO_2 after the reductive pretreatment are shown in figure 27 as a function of time, temperature and the CO/O_2 reactant feed ratio. An initial reaction temperature of 323 K was used, which was then stepwise (by increments of 30 K each, holding time 30 min) increased up to 453 K followed by stepwise decreasing the temperature to the initial temperature, continued by a second cycle. This temperature program was applied to all the CO oxidation measurements. Every increase in temperature resulted in an increase in the conversion of CO, which was then stable under isothermal conditions independent of the cycle number. This indicates that under the applied reaction conditions no (structural) deactivation of the catalyst occurs.

The degrees of CO conversion observed for the measurements with constant O_2 partial pressure (figure 27) are summarized in table 5. The highest degree of conversion of CO (80%) was observed for the CO/O_2 reactant feed ratio of 2.0. For the reactant feed ratios of 0.5 and 1.0 (i.e. under oxidizing conditions) the maximum conversion of CO was 72 and 78%, respectively; whereas 44.0 and 26.0% CO conversion were found for CO/O_2 reactant feed ratios of 4.0 and 6.0, respectively. It has to be mentioned that for the latter ratios

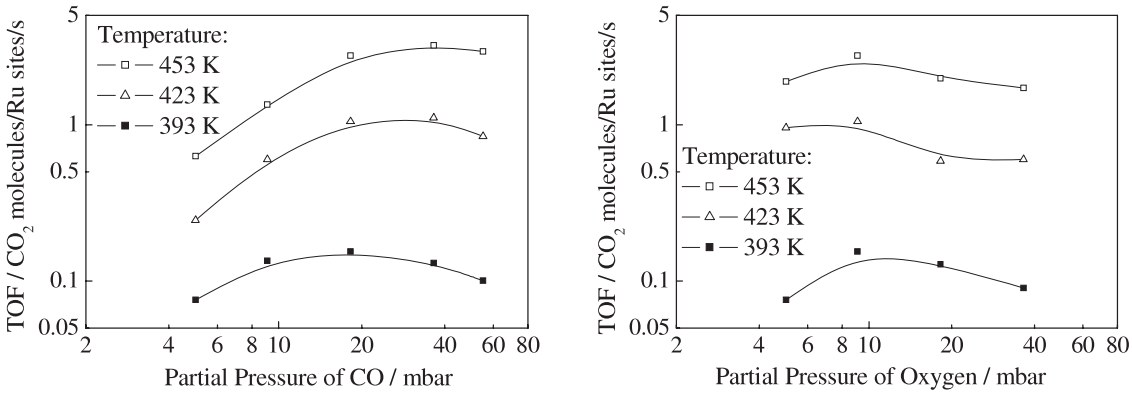

Figure 28. TOFs (CO_2 molecules formed per Ru site per second) measured for the oxidation of CO at three different temperatures over pre-reduced RuO_2/Ru as a function of the partial pressure of CO (left) and O_2 (right). The partial pressure of the second reactant was held constant: $O_2 = 9.1$ mbar (left), CO = 18.2 mbar (right).

Table 5. Steady-state degrees of CO conversion obtained for the oxidation of CO over 12.5 mg microscale pre-reduced RuO_2/Ru powder using a total feed of 50 N ml min^{-1}.

Partial pressure (mbar)		Conversion of CO (%) at different temperatures		
CO	O_2	393 K	423 K	453 K
4.5	9.1	6.2	34.0	72.0
9.1	9.1	6.0	34.0	78.0
18.2	9.1	5.0	30.0	81.0
36.4	9.1	1.5	14.1	44.0
54.7	9.1	1.0	7.1	26.0

(4 and 6) the maximum theoretical CO conversion is restricted to 50 and 33.3%, respectively.

Based on the steady-state degrees of conversion, it is possible to calculate turnover frequencies (TOF) and to derive reaction orders. TOFs as a function of the partial pressure of CO at constant O_2 pressure are shown in figure 28 as a function of the feed composition. for three different temperatures. At low partial pressures of CO and at a temperature of 393 K the reaction is of positive order in CO. The reaction changes to negative order, when the CO partial pressure was above 18 mbar, i.e. for $CO/O_2 > 2$.

An optimum rate of the reaction was observed near the stoichiometric 2:1 composition of the reactant feed. A closer inspection of figure 28 (left) indicates that the optimum reaction rate slightly shifts to higher partial pressures of CO at 423 and 453 K. A similar CO partial pressure dependence was reported for single-crystal model catalysts under both high pressure conditions at 500 K [4] and UHV conditions at 350 K [40].

TOFs as a function of the partial pressure of O_2 (at constant CO pressure) are shown in figure 28 (right) for three different temperatures. At low oxygen partial pressures and at 393 K the reaction is of positive order in oxygen, whereas for the same temperature but higher O_2 partial pressures the reaction is of negative order in oxygen. An optimum rate of the reaction was again observed near the stoichiometric composition of the reactant feed. However, at 423 and 453 K the reaction rate was almost zero order with respect to oxygen.

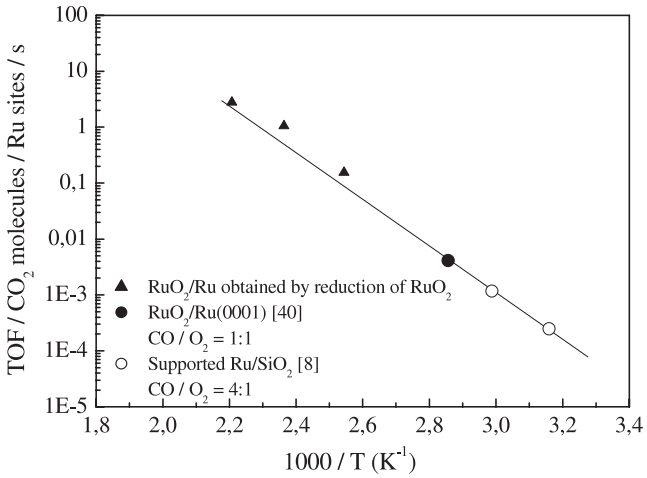

Figure 29. Arrhenius plot of turnover frequencies (CO_2 molecules formed per Ru site and second) measured for the oxidation of CO over RuO_2/Ru obtained by reduction of RuO_2. TOFs reported for $RuO_2(110)/Ru(0001)$ [40] and for SiO_2-supported Ru nanoparticles [8] are also included. Apparent activation energy derived from the Arrhenius plot: $E_A = 82$ kJ mol^{-1}.

This observation is also in agreement with the results reported for the RuO_2 single-crystal model catalysts [40].

In figure 29 the calculated turnover frequencies are shown in an Arrhenius plot. For comparison the TOFs reported for the CO oxidation over RuO_2 single-crystal surfaces [40] and supported Ru nanoparticles [8] are included. Independent of the material, extrapolation of the data reveals an excellent agreement. For the stable unsupported RuO_2/Ru catalyst the TOFs reveal slight variations even for measurements with a constant CO/O_2 reactant feed ratio. These variations can be explained by the reaction orders of the reactants, which were shown to be dependent on the CO/O_2 ratio as well as on the temperature.

It is remarkable that the optimum reaction rate for the oxidation of CO can be accomplished with just the stoichiometric ratio, whereas for an excess of O_2 or CO the corresponding reaction orders turn out to be negative leading to a decreasing reaction rate. Since we are not faced with the problem of deactivation of the pre-reduced polycrystalline

RuO_2/Ru catalyst, the maximum reaction rate for the stoichiometric reactant feed has to be traced to the reaction kinetics. Equations (1)–(3) describe the reaction mechanism by a set of three elementary steps. Although it has been shown (cf sections 4.2–4.4) that a mean-field approach is not suitable for a proper description of the kinetics, it is used here for providing qualitative information. Based on a variety of investigations summarized in this review, the reaction between adsorbed CO and adsorbed O atoms (equation (3)) can be assumed to be the rate determining step. Assuming a fast and non-activated competitive adsorption of CO and O_2 (step (1) and step (2)), the surface is supposed to be fully covered by the reactants in the temperature range up to 453 K [35].

$$CO + {}^* \rightarrow CO_{ads} - {}^* \tag{1}$$

$$O_2 + 2^* \rightarrow 2O_{ads} - {}^* \tag{2}$$

$$CO_{ads} + O_{ads} \rightarrow CO_2 + 2^*. \tag{3}$$

For full coverage ($\theta_{CO} + \theta_O = 1$) it follows from equation (4) that optimum reaction rates are reached for equal amounts of O_{ads} and CO_{ads}, and it is obvious that the maximum reaction rate corresponds to the stoichiometric reactant feed ratio, assuming similar pre-exponential adsorption factors for CO adsorption and dissociative O_2 adsorption.

$$\frac{dc_{CO_2}}{dt} = k \cdot \theta_{CO} \cdot \theta_O = k \cdot \theta_{CO} \cdot (1 - \theta_{CO}). \tag{4}$$

Furthermore, due to the full coverage only the reaction rate constant k in equation (4) depends on temperature, and, as a consequence, the apparent activation energy of 82 kJ mol^{-1} derived from figure 29 actually corresponds to the activation energy for the recombination of the adsorbed reactants (equation (3)) in this simplified model.

The ratio of coverages can be expressed as:

$$\frac{\theta_O}{\theta_{CO}} = \frac{2J_{O_2}s_O}{J_{CO}s_{CO}}$$

where J_j is the flux and s_j is the sticking coefficient of component j. Assuming that the two adsorption steps occur equally fast, that is, for non-activated adsorption and sticking coefficients of 1 the model yields a parabolic dependence of the reaction rate on the reactant feed ratio with a maximum at the stoichiometric composition.

It is obvious that our simple model fails, when the oxygen coverage approaches one (reaction rates near 0), requiring a full description of all elementary steps on the various sites and coverage-dependent sticking coefficients, as already indicated in the analysis of the O_2 TPD experiments (cf figure 6). In this way, a significantly better modeling of the kinetic data can be achieved [35].

5. Concluding remarks and outlook

The sustaining dream of '*ab initio*' catalysis (i.e. rational catalyst design) can only become true when applied catalysis (e.g. technical chemistry), surface chemistry together with *ab initio* theory coherently work on a particular catalyzed reaction system. So far only very few successful examples have been reported in the literature and most of these examples originate from Denmark, where physics and chemistry groups from Danish universities and the R&D department of Haldor Topsøe, a leading catalyst company, run a successful network of catalysis [73–75].

Here we have presented another example how such a close cooperation can lead to a successful bridging of the pressure and materials gaps and to an improved catalyst based on the atomic scale understanding gained by this bridging process:

(a) For nanoscale RuO_2 powder it was found that this catalyst is able to accommodate additional adsorbed oxygen which desorbs around 450–500 K. The polycrystalline RuO_2 powder was cleaned by heating in flowing He to 523 K and additional gentle oxidative purification in flowing O_2 at 423 K followed by cooling in O_2 to room temperature. The O_2 TPD spectrum is practically identical to that of the single-crystalline RuO_2(110) surface. In addition, from the total amount of desorbed O_2 and the known catalyst dispersion, the coverage of on-top oxygen was estimated to be 70%, close to the saturation coverage found for RuO_2(110). This experiment indicates clearly that the active polycrystalline RuO_2 powder surfaces expose the same onefold coordinatively unsaturated Ru sites as on single-crystalline RuO_2 films.

(b) *In situ* RAIRS experiments of RuO_2(110) indicate stable spectra in the pressure range of 10^{-6}–10^{-3} mbar which are very similar to those obtained by DRIFTS for supported Ru catalyst under higher pressures but with the same constitution of the reactant feed. This demonstrates that under reaction conditions the active phase both for the model catalyst and the supported practical catalyst is RuO_2.

(c) The TOF of polycrystalline RuO_2 catalysts and of the single-crystalline RuO_2(110) surface agree very well (cf figure 29).

(d) Even the proposed core–shell model for the active and stable powder RuO_2/Ru catalyst is fully reconciled with the self-limiting growth of a 1.6 nm thick RuO_2(110) film on Ru(0001) in a wide pressure and temperature range.

(e) Microkinetic modeling of the CO oxidation data over polycrystalline RuO_2/Ru powder provides an activation barrier which is determined by the recombination step of adsorbed CO and O on the catalyst surface amounting to 82 kJ mol^{-1} in almost perfect agreement with that of single-crystalline RuO_2(110) data [40] and theoretical data [62, 63, 66].

(f) The close interplay of the surface science approach with the research on practical catalysts provided a synergistic strategy to improve the performance of applied Ru-based catalysts [21, 22, 30]. For the case of ruthenium, we explained the microscopic processes determining the structural deactivation of ruthenium-based catalysts while oxidizing CO under net oxidizing reaction conditions. Based on this atomic scale knowledge stable and active applied Ru catalysts can be designed. For instance, RuO_2 powder catalyst must first be reduced with H_2 at 773 K and subsequently mildly re-oxidized at 450 K, resulting in RuO_2/Ru core–shell particles with an ultrathin RuO_2 film coating the metal core.

As outlined in the introduction, the high catalytic activity of Ru(0001) in the CO oxidation reaction at higher pressures found by Peden and Goodman [4] has initiated the RuO_2 work fifteen years later [5]. Although RuO_2 is indeed a remarkable active oxidation catalyst, and that not only for the CO oxidation reaction, the high catalytic activity found in Goodman and Peden's work [4] is still not well understood [76]. Even under the most strongly oxidizing reaction condition where pure oxygen is supplied in the reactant feed, the oxidation of Ru to RuO_2 metal takes place only for temperatures higher than about 500 K. This threshold temperature was found for single-crystalline Ru(0001) [11, 77] and for 7 nm thick nanocrystalline Ru films on Si [31]. Since most of the experiments in [4] were performed at temperatures below this threshold temperature, RuO_2 may not be the catalytically active phase. However, for temperatures above 500 K oxide formation on the Ru(0001) is possible, and for the particular reaction condition in [11] the oxidation of Ru(0001) was shown by *in situ* SXRD to take place at 650 K. It is still quite surprising that the activation barrier found by Peden and Goodman (82 kJ mol^{-1}) is identical to that found on RuO_2(110). We should mention that under typical CO oxidation reaction conditions supported Ru catalysts do even oxidize at room temperature, since the reaction heat drives the catalyst beyond the threshold temperature [9]. Therefore, the RuO_2 phase is decisive to explain the high activity of supported Ru catalysts under realistic CO oxidation reaction conditions. Below the oxidation threshold temperature of 500 K Blume *et al* [77] suggested that a non-stoichiometric transient surface oxide (TSO) is the active phase in the catalytic CO oxidation over Ru(0001). The TSO may be able to explain Peden and Goodman's data.

Since the year 2000 RuO_2 has evolved from a pure target of fundamental research into a promising practical catalyst with a wide range of potential applications. The simple CO oxidation reaction, for instance, can be catalyzed even at room temperature and in humid environment. This allows for zero-energy air purification [78]. RuO_2 is also considered as a potential electrocatalyst for low temperature fuel cells [79] and is the best anode catalyst known today for the electrochemical water splitting [80]. Further applications of RuO_2 are found in the field of 'green chemistry'. The oxidative dehydrogenation of simple alcohols proceeds already at low temperatures [81]. The first chemical plant for the low temperature oxidation of HCl, which is based on the catalyst RuO_2, was erected by the Sumitomo Chemicals Cooperation in 2004 [82]. While metallic Ru is an excellent catalyst for ammonia synthesis, RuO_2 turned out to be a promising catalyst for the oxidation of ammonia to NO at relatively low temperatures of 550 K [83] compared to 1000–1200 K for standard Rh-stabilized Pt gauzes [84]. Furthermore supported RuO_2 on alumina efficiently catalyzes the oxidation of primary and secondary amines to form nitriles and imines [85]. But also the direct combustion of carbon can be performed with RuO_2 at substantially lower temperatures than with alternative catalysts [86]. This process may find application for the automotive exhaust purification of diesel engines.

All these applications of RuO_2 have in common that RuO_2 is active for the total and partial oxidation reactions at low temperatures. A very different application of RuO_2 (and much more attractive to physicists) is related to extreme ultraviolet lithography (EUVL), the leading candidate for the next-generation lithography to be used in semiconductor manufacture [87]. One of the major challenges to be met in EUVL is the lifetime of the imaging reflection optics, usually consisting of alternating Si/Mo multilayers. The combination of exposure to high intensity EUV radiation and the presence of hydrocarbons and water in the residual gas leads to fast degradation of optical reflectivity due to oxidation and growth of carbon multilayers [88]. Ruthenium-based capping layers of 2–3 nm thickness have been promising for protection of the Mo–Si multilayer systems. Although they also undergo oxidation and carbon contamination in typical EUV environment the degradation of the optical reflectivity is significantly slowed down [89]. The excellent catalytic activity of Ru and respectively RuO_2 can be exploited for the removal of carbonaceous contaminations [90]. Here catalysis meets EUV lithography, an exciting interdisciplinary research field [91].

Acknowledgments

We gratefully acknowledge financial support by the Deutsche Forschungsgemeinschaft (DFG, SPP 1091) and fruitful discussions with Professor Dr Gerhard Ertl. We thank the Leibniz-Rechenzentrum in Munich for providing us with massive parallel computing time. Partial financial support is acknowledged from the European Union under contract no. NMP3-CT-2003-505670 (NANO2) and Intel Corp.

References

[1] Thomas J M and Thomas W J 1997 *Principles and Practice of Heterogeneous Catalysis* (Weinheim: VCH)
[2] Duke C B and Plummer E W (eds) 2001 Frontiers in surface and interface science *Surf. Sci.* **500**
[3] Ertl G, Knözinger H and Weitkamp J (ed) 1997 *Handbook of Heterogeneous Catalysis* (Weinheim: VCH)
[4] Peden C H F and Goodman D W 1986 *J. Phys. Chem.* **90** 1360
[5] Over H, Kim Y D, Seitsonen A P, Wendt S, Lundgren E, Schmid M, Varga P, Morgante A and Ertl G 2000 *Science* **287** 1474–6
[6] Hinrichsen O, Rosowski F, Muhler M and Ertl G 1996 *Chem. Eng. Sci.* **51** 1683
[7] Bielawa H, Hinrichsen O, Birkner A and Muhler M 2001 *Angew. Chem. Int. Edn* **40** 1061
[8] Aßmann J, Löffler E, Birkner A and Muhler M 2003 *Catal. Today* **85** 235
[9] Narkhede V, Aßmann J and Muhler M 2005 *Z. Phys. Chem.* **219** 979–95
[10] Kim Y D, Seitsonen A P and Over H 2000 *Surf. Sci.* **465** 1
[11] He Y B, Knapp M, Lundgren E and Over H 2005 *J. Phys. Chem.* B **109** 21825
[12] Kim Y D, Seitsonen A P, Schwegmann S and Over H 2001 *J. Phys. Chem.* B **105** 2205
[13] Lindroos M, Pfnür H, Held G and Menzel D 1989 *Surf. Sci.* **222** 451
Pfnür H, Held G, Lindroos M and Menzel D 1989 *Surf. Sci.* **220** 43
[14] Kostov K L, Gsell M and Jacob P 1997 *Surf. Sci.* **394** L138
Kim Y D, Wendt S, Schwegmann S, Over H and Ertl G 1998 *Surf. Sci.* **418** 267

[15] Stampfl C, Schwegmann S, Over H, Scheffler M and Ertl G 1996 *Phys. Rev. Lett.* **77** 3371–4
[16] Böttcher A and Niehus H 1999 *Phys. Rev.* B **60** 14396–404
[17] Over H and Seitsonen A P 2002 *Science* **297** 2003–4
[18] Böttcher A, Starke U, Conrad H, Blume R, Niehus H, Gregoratti L, Kaulich B, Barinov A and Kiskinova M 2002 *J. Chem. Phys. Chem.* **117** 8104
[19] Blume R, Hävecker M, Zafeiratos S, Teschner D, Knop-Gericke A, Schlögl R, Lizzit S, Dudin P, Barinov A and Kiskinova M 2007 *Phys. Chem. Chem. Phys.* **6** 3648
[20] Over H, Kim Y D, Seitsonen A P, Wendt S, Lundgren E, Schmid M, Varga P, Morgante A and Ertl G 2000 *Science* **287** 1474–6
[21] Knapp M, Seitsonen A P, Kim Y D and Over H 2004 *J. Phys. Chem.* **108** 14392–7
[22] Aßmann J, Crihan D, Knapp M, Lundgren E, Löffler E, Muhler M, Narkhede V, Over H, Schmid M and Varga P 2005 *Angew. Chem. Int. Edn* **116** 939–42
[23] Over H, Seitsonen A P, Lundgren E, Smedh M and Andersen J N 2002 *Surf. Sci.* **504** 196
[24] Over H, Seitsonen A P, Lundgren E, Schmid M and Varga P 2002 *Surf. Sci.* **515** 143–56
[25] Kim Y D, Over H, Krabbes G and Ertl G 2001 *Top. Catal.* **14** 95–100
[26] Kim Y D, Seitsonen A P, Wendt S, Wang J, Fan C, Jacobi K, Over H and Ertl G 2001 *J. Phys. Chem.* B **105** 3752–8
[27] Over H, Seitsonen A P, Knapp M, Lundgren E, Schmid M and Varga P 2004 *Chem. Phys. Chem.* **5** 167–74
[28] Seitsonen A P and Over H 2002 Ruthenium dioxide, a versatile oxidation catalyst: first principle analysis *High Performance Computing in Science and Engineering in Munich* (Berlin: Springer) pp 171–80
[29] Korte C 2006 unpublished ESBD measurements
[30] Aßmann J, Narkhede V, Löffler E, Hinrichsen O, Over H and Muhler M 2004 *J. Phys. Chem.* B **108** 14634–42
[31] He Y B, Goriachko A, Korte C, Farkas A, Mellau G, Dudin P, Gregoriatti L, Barinov A, Kiskinova M, Stierle A, Kasper N, Bajt S and Over H 2007 *J. Phys. Chem.* C **111** 10988
[32] Falconer J L and Schwarz J A 1983 *Catal. Rev. Sci. Eng.* **25** 141
[33] Christmann K 1991 *Introduction to Surface Physical Chemistry* (Darmstadt: Steinkopff)
[34] Wendt S 2002 *PhD Thesis* FU Berlin
[35] Breuer N A and Muhler M 2008 *J. Catal.* to be submitted
[36] Wang H and Schneider W F 2007 *J. Chem. Phys.* **127** 064706
[37] Seitsonen A P, Kim Y D, Knapp M, Wendt S and Over H 2002 *Phys. Rev.* B **65** 035413–21
[38] Farkas A, Mellau G and Over H 2008 RAIRS experiments at press
[39] Fan C Y, Wang J, Jacobi K and Ertl G 2001 *J. Chem. Phys.* **114** 10058–63
[40] Wang J, Fan C Y, Jacobi K and Ertl G 2002 *J. Phys. Chem.* B **106** 3422–7
[41] Cant N W, Hicks P C and Lennon B S 1978 *J. Catal.* **54** 372–9
[42] Kiss J T and Gonzalez R D 1984 *J. Phys. Chem.* **88** 892
[43] Over H and Muhler M 2003 Catalytic CO oxidation over ruthenium—bridging the pressure gap *Prog. Surf. Sci.* **72** 3–17
[44] Ackermann M D *et al* 2005 *Phys. Rev. Lett.* **95** 255505
[45] Paulus U A, Wang Y, Kim S H, Geng P, Wintterlin J, Jacobi K and Ertl G 2004 *J. Chem. Phys.* **121** 11301
[46] Assmann J, Narkhede V and Muhler M 2004 unpublished results
[47] Kim Y D, Seitsonen A P and Over H 2001 *Phys. Rev.* B **63** 5419–25
[48] Rössler M, Günther S and Wintterlin J 2007 *J. Phys. Chem.* C **111** 2242
[49] Lobo A and Conrad H 2003 *Surf. Sci.* **523** 279
[50] Madhavaram H, Idriss H, Wendt S, Kim Y D, Knapp M, Over H, Aßmann J, Löffler E and Muhler M 2001 *J. Catal.* **202** 296–307
[51] Wang Y, Lafosse A and Jacobi K 2002 *J. Phys. Chem.* B **106** 5476–82
[52] Wang Y, Jacobi K and Ertl G 2003 *J. Phys. Chem.* B **107** 13918–24
[53] Paulus U A, Wang Y, Bonzel H P, Jacobi K and Ertl G 2005 *J. Phys. Chem.* B **109** 2139
[54] Wang Y, Jacobi K, Schöne W-D and Ertl G 2005 *J. Phys. Chem.* B **109** 7883
[55] Over H 2002 Ruthenium dioxide, a fascinating material for atomic scale chemistry *Appl. Phys.* A **75** 37–44
[56] Wang J, Fan C Y, Sun Q, Reuter K, Jacobi K, Scheffler M and Ertl G 2003 *Angew. Chem. Int. Edn* **42** 2151
[57] Knapp M, Crihan D, Seitsonen A P and Over H 2005 *J. Am. Chem. Soc.* **127** 3236–7 (Communication to the Editor)
[58] Knapp M, Crihan D, Seitsonen A P, Lundgren E, Resta A, Andersen J N and Over H 2007 *J. Phys. Chem.* C **111** 5363–73
[59] Crihan D, Knapp M, Seitsonen A P and Over H 2006 *J. Phys. Chem.* B **110** 22947
[60] Over H, Seitsonen A P, Lundgren E, Schmid M and Varga P 2001 *J. Am. Chem. Soc.* **123** 11807 (Communication to the Editor)
[61] Liu Z-P, Hu P and Alavi A 2001 *J. Chem. Phys.* **114** 5957–8
[62] Wendt S, Seitsonen A P, Kim Y D, Knapp M, Idriss H and Over H 2002 *Surf. Sci.* **505** 137–52
[63] Wendt S, Seitsonen A P and Over H 2003 *Catal. Today* **85** 167–75
[64] Wendt S, Knapp M and Over H 2004 *J. Am. Chem. Soc.* **126** 1537–41
[65] Kresse G and Furthmüller J 1996 *Comput. Mater. Sci.* **6** 15
Kresse G and Furthmüller J 1996 *Phys. Rev.* B **54** 11169
Blöchl P E 1994 *Phys. Rev.* B **10** 17953
Kresse G and Joubert J 1999 *Phys. Rev.* B **59** 1758
[66] Kliejna A, Kresse G, Rogal J, De Sarkar A, Reuter K and Scheffler M 2006 *Phys. Rev.* B **73** 035404
[67] Chorkendorff I and Niemantsverdriet J W 2003 *Concepts of Modern Catalysis and Kinetics* (New York: Wiley)
[68] Reuter K and Scheffler M 2003 *Phys. Rev.* B **68** 045407
[69] Gong X-Q, Liu Z-P, Raval R and Hu P 2004 *J. Am. Chem. Soc.* **126** 8
Liu Z-P, Hu P and Alavi A 2001 *J. Chem Phys.* **114** 5956
[70] Seitsonen A P and Over H 2008 at press
[71] Reuter K and Scheffler M 2006 *Phys. Rev.* B **73** 045433
[72] Reuter K, Frenkel D and Scheffler M 2004 *Phys. Rev. Lett.* **93** 116105
[73] Besenbacher F, Chorkendorff I, Clausen B S, Hammer B, Molenbroek A M, Norkov J K and Steensgaard I 1998 *Science* **279** 1913
[74] Jabobsen C J H, Dahl S, Clausen B S, Bahn S, Logadottir A and Norskov J N 2001 *J. Am. Chem. Soc.* **123** 8404
[75] Hansen T W, Wagner J B, Hansen P L, Dahl S, Topsøe H and Jacobsen C J H 2001 *Science* **294** 1508
[76] Goodman D W, Peden C H F and Chen M S 2007 *Surf. Sci.* **601** L124
Over H, Muhler M and Seitsonen A P 2007 *Surf. Sci.* **601** 5659 comment on this paper
[77] Blume R, Hävecker M, Zafeiratos S, Teschner D, Kleimenov E, Knop-Gericke A, Schlögl R, Barinov A, Dudin P and Kiskinova M 2006 *J. Catal.* **239** 345
[78] Zang L and Kisch H 2000 *Angew. Chem.* **112** 4075
Zang L and Kisch H 2000 *Angew. Chem. Int. Edn* **39** 3921
[79] Lin W F, Jin J M, Christensen P A and Scott K 2003 *Electrochim. Acta* **48** 3815–22
[80] Trasatti S 1991 *Electrochim. Acta* **36** 225
[81] Liu H and Iglesia E 2005 *J. Phys. Chem.* B **109** 2155–63

[82] Seki K, Iwanaga K and Hibi T 2005 Improved hydrogen chloride oxidation process: characterization of the RuO_2/TiO_2 catalyst *INOR-233 229th ACS National Meeting (San Diego, CA, March 2005)* (Abstracts of Papers)
[83] Wang Y, Jacobi K, Schöne W D and Ertl G 2005 *J. Phys. Chem.* B **109** 7883
[84] Baerns M, Imbihl R, Kondratenko V A, Kraehnert R, Offermans W K, van Santen R A and Scheibe A 2005 *J. Catal.* **232** 226
[85] Yamaguchi K and Mizuno N 2003 *Angew. Chem.* **115** 1518
[86] Villain K, Kirschhock C E A, Martens J A, Liang D and Van Tendeloo G 2006 *Angew. Chem. Int. Edn* **45** 3106
[87] Baijt S, Alameda J B, Barbee T W Jr, Clift W M, Folta J A, Kaufman B and Spiller E A 2002 *Opt. Eng.* **41** 1797
[88] Mertens B, Weiss M, Meiling H, Klein R, Louis E, Kurt R, Wedowski M, Trenkler H, Wolschrijn B, Jansen R, van de Runstraat A, Moors R, Spee K, Plöger S and Van de Kruijs R 2004 *Microelectron. Eng.* **73/74** 16
[89] Borodovsky Y 2006 *Proc. SPIE* **6153** 615302
[90] Montcalm C, Bajt S, Mirkarimi P B, Spiller E, Weber F J and Folta J A 1998 *Proc. SPIE* **3331** 42
[91] Over H, He Y B, Farkas A, Mellau G, Korte C, Knapp M, Chandhok M and Fang M 2007 *J. Vac. Sci. Technol.* B **25** 1123